The Framework for Assessing Changes To Sea-level (FACTS) v1.0-rc: A platform for characterizing parametric and structural uncertainty in future global, relative, and extreme sea-level change

Robert E. Kopp[1,2], Gregory G. Garner[1,2,*], Tim H. J. Hermans[3,4], Shantenu Jha[2,5,6], Praveen Kumar[1,2], Aimée B.A. Slangen[3], Matteo Turilli[5,6], Tamsin L. Edwards[7], Jonathan M. Gregory[8,9], George Koubbe[5], Anders Levermann[10], Andre Merzky[5], Sophie Nowicki[11], Matthew D. Palmer[8,12], and Chris Smith[13,14]

[1]Department of Earth and Planetary Sciences, Rutgers University, Piscataway, NJ, USA
[2]Rutgers Institute of Earth, Ocean, and Atmospheric Sciences, Rutgers University, New Brunswick, NJ, USA
[3]NIOZ Royal Netherlands Institute for Sea Research, Department of Estuarine & Delta Systems, Utrecht University, PO Box 140, 4400 AC Yerseke, The Netherlands
[4]Utrecht University, Institute for Marine and Atmospheric research Utrecht (IMAU), Utrecht, The Netherlands
[5]Department of Electrical and Computer Engineering, Rutgers University, Piscataway, NJ, USA
[6]Computational Science Initiative, Brookhaven National Laboratory, Upton, NY, USA
[7]Department of Geography, King's College London, London, UK
[8]Met Office Hadley Centre, Exeter, UK
[9]National Centre for Atmospheric Science, University of Reading, Reading, UK
[10]Potsdam Institute for Climate Impact Research, Potsdam, Germany
[11]University at Buffalo, Buffalo, NY, USA
[12]University of Bristol, School of Earth Sciences, Bristol, UK
[13]Priestley International Centre for Climate, University of Leeds, UK
[14]International Institute for Applied Systems Analysis (IIASA), Laxenburg, Austria
[*]Current affiliation: Gro Intelligence, New York, NY, USA

Correspondence: Robert E. Kopp (robert.kopp@rutgers.edu)

Abstract. Future sea-level rise projections are characterized by both quantifiable uncertainty and unquantifiable, structural uncertainty. Thorough scientific assessment of sea-level rise projections requires analysis of both dimensions of uncertainty. Probabilistic sea-level rise projections evaluate the quantifiable dimension of uncertainty; comparison of alternative probabilistic methods provide an indication of structural uncertainty. Here we describe the Framework for Assessing Changes To Sea-level (FACTS), a modular platform for characterizing alternative probability distributions of global mean, regional, and extreme sea-level rise. We demonstrate its application by generating seven alternative probability distributions under multiple alternative emissions scenarios for both future global mean sea level and future relative and extreme sea level at New York City. These distributions, closely aligned with those presented in the Intergovernmental Panel on Climate Change Sixth Assessment Report, emphasize the role of the Antarctic and Greenland ice sheet as drivers of structural uncertainty in sea-level rise projections.

1 Introduction

Quantitative projections of future sea-level change have been of interest to both scientists and decision-makers since at least the 1980s (Garner et al., 2018; Hall et al., 2019; Horton et al., 2018; Kopp et al., 2019). To our knowledge, the first peer-reviewed
15   scientific article projecting 21st century global mean sea-level rise appeared in *Science* in 1982 (Gornitz et al., 1982); the first planning-oriented sea-level scenarios in the United States were adopted by the US Army Corps of Engineers in 1986 (US Army Corps of Engineers, 1986), associated with a National Research Council study published in 1987 (National Research Council, 1987). Thus, sea-level projections have always been one of the more practically relevant parts of scientific assessments of climate change, including all six of the Intergovernmental Panel on Climate Change (IPCC) Working Group 1 reports (Kopp
20   et al., in review).

    At the same time, scientific projections of sea-level rise have also long acknowledged the presence of factors – particularly associated with Antarctic ice-sheet instability – that limit the ability to generate quantitative sea-level projections (e.g., Mercer, 1978; Gornitz et al., 1982). These limits give rise to what is sometimes called ambiguity or deep uncertainty – uncertainty that cannot be represented by singular probability distributions, due to limited amount, reliability, and unanimity of informa-
25   tion (ambiguity as defined by Ellsberg, 1961) or, similarly, to ignorance or disagreement among analysts (subtypes of deep uncertainty as defined by Lempert et al., 2003). The question of how to integrate such ambiguity into the assessment and communications of sea-level projections has long challenged the authors of scientific assessments (Oppenheimer et al., 2019b; Kopp et al., in review).

    Until about fifteen years ago, comprehensive, localized relative sea-level (RSL) projections were uncommon (e.g., Katsman
30   et al., 2008; National Research Council, 2012). Many users simply augmented global mean sea level (GMSL) projections with estimates of land subsidence to project local relative sea level RSL change. The IPCC Fourth Assessment Report considered only deviations from GMSL driven by sterodynamics (see Gregory et al. (2019) for sea level terminology) and represented in coupled atmosphere-ocean general circulation models (Meehl et al., 2007). Other researchers focused on the gravitational, rotational, and deformational (GRD) relative sea level changes caused by redistributing mass within the cryosphere and hydro-
35   sphere (e.g., by melting land ice) (e.g., Mitrovica et al., 2009). The IPCC Fifth Assessment Report was the first IPCC report to consider both sterodynamic sea level and GRD, along with the effects of glacial isostatic adjustment, in its relative sea-level projections (Church et al., 2013).

    The AR5 projections and numerous subsequent studies taking on this challenge (Fox-Kemper et al., 2021) are generally referred to as 'probabilistic' projections, in that, under different emissions scenarios, they estimate probability distributions
40   for the change in each of the driving factors of GMSL and RSL change and their total. Producing such projections require combining different lines of information: global climate models (GCMs) can simulate thermal expansion and sterodynamic sea level, but do not in general include coupled glaciers, ice sheets, or anthropogenic changes in land water storage. They also require using relatively simple representations of core elements; models of the complexity of GCMs do not lend themselves to the Monte Carlo sampling used to estimate sea-level distributions in these studies. The ProjectSL/LocalizeSL framework
45   developed by Kopp et al. (2014, 2017) is one commonly used example of a probabilistic sea-level projection framework.

Probabilistic sea-level projection frameworks are limited in that they assume that future changes under a single emissions scenario can be represented by single probability distribution. This assumption is not in general true for processes characterized ambiguity (Kopp et al., in review; Hinkel et al., 2019). While some studies (e.g. Kopp et al., 2017; Jevrejeva et al., 2019) have worked around this problem to explore structural uncertainties by substituting in different modeling approaches for different
50   components, probabilistic projection frameworks have not generally been engineered to facilitate such explorations.

This paper describes the Framework for Assessing Changes To Sea-level (FACTS), a scalable, modular, open-source framework for global mean, local, and extreme sea-level projection that is designed to support the characterization of ambiguity in sea-level projections. FACTS is built using modern computational practices and in the spirit of FAIR (Findable, Accessible, Interoperable, Reusable) science (Wilkinson et al., 2016). It is designed so users can easily explore deep uncertainty by investi-
55   gating the implications for GMSL, RSL, and extreme sea level (ESL) of different choices for different processes. Its modularity allows components to be represented by either simple or complex models. Because it is built upon the RADICAL-Cybertools computing stack (Merzky et al., 2021), different modules can in principle be dispatched for execution on resources appropriate to their computational complexity.

FACTS is, specifically, a tool for sea-level *assessment*. It is not intended as a substitute for detailed, process-based analyses
60   of individual sea-level contributions (for example, GCM studies of ocean dynamics, or ice-sheet modeling studies) or of integrated projections made with high-complexity Earth system models that are moving toward including coupled ice sheets (e.g., Muntjewerf et al., 2021; Smith et al., 2021). Such studies provide the scientific bases underlying FACTS modules. Rather, FACTS is intended to support scientists – like those participating in the IPCC and in numerous national and subnational assessment processes – who seek to develop projections that are internally consistent, represent the richness of approaches
65   present in the scientific literature, and assess multiple types of uncertainty. Such assessment outputs, rather than individual projections in the primary scientific literature, are generally the primary way in which climate risk practitioners interact with estimates of future sea-level change (Kopp et al., in review).

Development versions of FACTS modules underlie the GMSL and RSL projections of the IPCC Sixth Assessment Report (AR6) (Fox-Kemper et al., 2021; Slangen et al., in press) and the 2022 US Government sea-level rise Technical Report (Sweet
70   et al., 2022). For these implementations, several key steps were run offline, and modules were invoked outside the execution and data management framework provided by the FACTS Manager. FACTS 1.0 allows replication of the AR6 approach entirely within FACTS, starting from specification of emissions scenarios and ending with the production of multiple, alternative probability distribution for GMSL, RSL and ESL.

2   Model Description

2.1   Overview

FACTS consists of the FACTS Manager, which oversees the execution of FACTS experiments, and an extendable suite of modules, which provide the scientific and analytical core that allow FACTS to simulate the different process contributing to global, local, and extreme sea level. Modules represent independent processes (e.g., sterodynamics or vertical land motion)

and can be run in parallel on high-performance computing (HPC) resources. Modules can also be run in sequence when their
outputs depend upon inputs from other modules (e.g., the modules that compute total relative sea-level change and extreme
sea-level distribution shifts).

A FACTS experiment consists of a series of Experiment Steps (Figure 1). Typical Experiment Steps include: (1) a climate
step, which translates an inputted emissions scenario into projections of global mean surface air temperature and ocean heat
content change; (2) a sea level components step, which simulates the different physical processes driving sea level change; (3)
an integration step, which adds up the different components into projections of total GMSL and RSL change; and (4) an ESL
step, which uses tide gauge data and RSL projections to project the change in extreme sea level occurrences over time.

Each step runs one or more modules in parallel. Exchange of information between modules happens in between steps. This
exchange is mediated by the file system, so steps can be bypassed simply by providing appropriate input files (e.g, stored
temperature and ocean heat content trajectories) to the subsequent step. Though the existing usage of FACTS contains only
one sea level component step, and therefore treats the output of each module as independent conditional upon their common
dependence on the climate simulated in the climate step, the FACTS Manager allows steps to be subdivided and thus could
support between-module coupling.

The core concept of Workflow provides FACTS with the flexibility required to explore structural uncertainty. A Workflow
consists of a set of sea level component modules that are added together in the integration step to produce a probabilistic
estimate of total sea level change. Workflows can be overlapping: for example, two Workflows might use the same module for
simulating sterodynamic sea level change, but use different modules for simulating ice sheet change. Modules run in the sea
level components step are tagged as belonging to one or more Workflows; those Workflows are then aggregated at the integra-
tion step. This structure allows a single sea level components step to include multiple modules representing alternative methods
to simulate the same sea level component and avoids redundant execution of modules employed in multiple Workflows.

In practice, for a specific set of climate inputs (e.g., emissions scenario-forced temperature projections), a single Workflow
produces a single (climate input-conditional) probabilistic projection of sea-level change. Multiple Workflows can be compared
to examine the structural uncertainty of GMSL, RSL, and ESL change to the choice of component methods (i.e., the ambiguity
of projections) and combined to produce summary outputs that capture ambiguity (Kopp et al., in review).

2.2 FACTS Manager and RADICAL-Cybertools

Though most of the FACTS modules implemented to date can be run on a desktop computer, and all can run on small-scale
high-performance computing clusters, FACTS is designed to allow modules of a broad range of computational demands,
including those requiring supercomputer resources. This objective is achieved by using the RADICAL-Cybertools software
stack in the FACTS Manager.

RADICAL-Cybertools are software systems designed specifically to support the extreme scale execution of applications
comprised of multiple tasks. A task can be any executable or Python function/method; tasks can have short ($\mathcal{O}$(seconds)) or
long ($\mathcal{O}$(hours to days)) duration; single/multiple core/GPU, single/multiple nodes, and single/multiple thread or MPI/OpenMP.
RADICAL-Cybertools are comprised of three existing systems: RADICAL Ensemble-Toolkit (hereafter, EnTK) (Balasubra-

manian et al., 2016, 2018), RADICAL-Pilot (Merzky et al., 2021) and RADICAL-SAGA (Merzky et al., 2015). From a software design perspective, RADICAL-Cybertools are software systems designed and implemented in accordance with the

115 building blocks approach (Turilli et al., 2019). Each system is independently designed with well-defined entities, functionalities, states, events and errors. Further, RADICAL-Cybertools can be integrated among themselves and with third-party middleware systems.

EnTK is the top-level system of the middleware stack used to implement FACTS. EnTK is an ensemble execution system, implemented as a Python library, that offers components to encode and execute ensemble applications on HPC systems. EnTK

120 uses RADICAL-Pilot (RP) to decouple the description of ensemble applications from their execution, separating three concerns: (i) specification of tasks and resource requirements; (ii) resource selection and acquisition; and (iii) management of task execution. EnTK sits between the user and the HPC system(s), abstracting resource and execution management complexities from the user.

EnTK exposes an API with three user-facing constructs: Pipeline, Stage, and Task. Those constructs allow the user to encode

125 an ensemble application in terms of concurrency and sequentiality of tasks. An Ensemble is a set or sequence of Pipelines, where each Pipeline is a sequence of Stages, and each Stage is a set of Tasks. Consistent with their formal definition, EnTK executes the members of a set concurrently and the members of a sequence sequentially. For example, all the Stages of each Pipeline execute sequentially, and all the Tasks of each stage execute concurrently. In this way, EnTK describes an ensemble application in terms of the concurrency and sequentiality of tasks, without requiring the explicit specification of tasks' data or

130 control dependencies.

EnTK manages failures of Tasks, components and RP. Failed Tasks can be resubmitted or ignored, depending on user configuration. By design, EnTK is resilient against its components failure as all state updates are transactional: failed components can be restarted without loss of information. RP is considered a black box and partial failures of its components at runtime are assumed to be handled locally. Upon full failure of RP, EnTK assumes all the resources and the tasks undergoing execution are

135 lost. EnTK starts a new instance of RP, acquiring new resources and resuming execution of the pipeline, stage, and tasks that had not previously successfully terminated.

In the context of the FACTS Manager, each Experiment Step is a set of Pipelines. Each Pipeline is associated with one FACTS module, and each module runs a series of sequential, single-task Stages described in its configuration file. Most typically, these stages consist of: (1) a pre-processing stage with a task that prepares associated data; (2) a fitting stage with a task that calibrates

140 the module based on the data prepared by the pre-processing stage; (3) a projection stage; and (4) a post-processing stage. Note that alternative specifications are possible, e.g., the totaling module runs in a single stage.

2.3 Modules

FACTS 1.0 includes a library of different modules (Table 1) that both illustrate functionality and allow simulation of projection work flows analogous to those employed in the IPCC Sixth Assessment Report (Fox-Kemper et al., 2021). Each of the included

145 modules is described below.
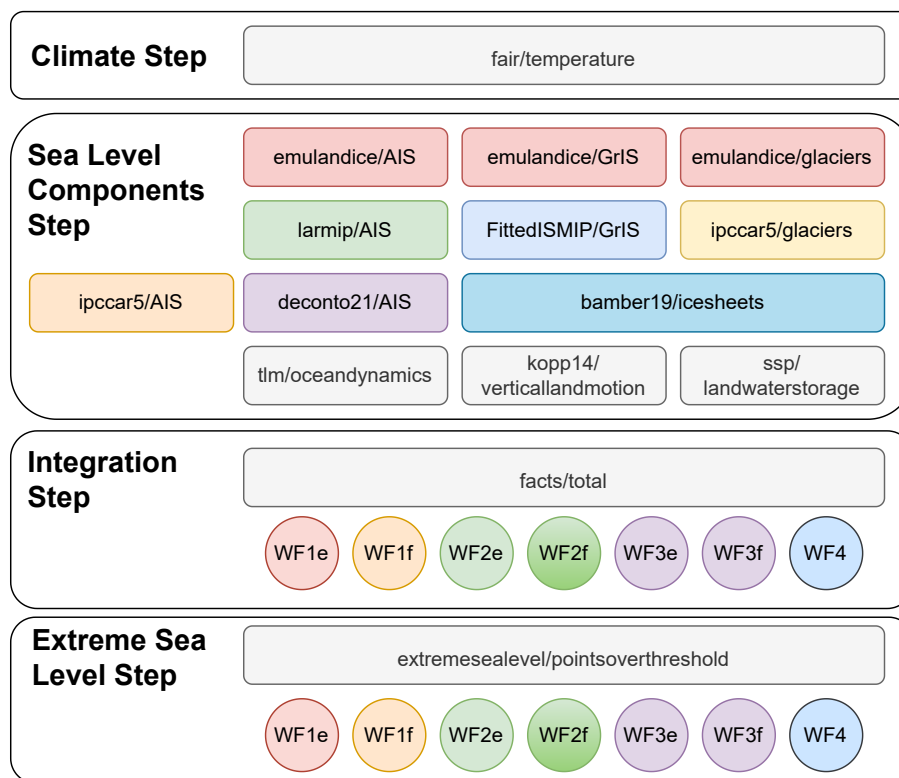
Figure 1. Schematic illustration of a FACTS experiment. Large boxes represent the four Experiment Steps. Smaller boxes represent different modules that might be run in each step. Circles represent Workflows generated by combining sets of sea level component modules in the integration step (and carried forward to the extreme sea-level step). Grey modules are applied to/included in all Workflows, while colored modules are included in some but not all Workflows in different combinations. See Table 2 for details of the modules making up each Workflow.

2.3.1 Climate module

Climate simulation is provided by the `fair/temperature` module. This module wraps around the FAIR v1.6.4 climate model emulator (Smith et al., 2018; Millar et al., 2017). Taking an emissions scenario as an input, this module samples uncertainty in key climate model parameters (e.g., equilibrium climate sensitivity and transient climate response) and generates probability distributions of global mean surface air temperature and ocean heat content. The climate simulation step can also be bypassed by providing to the modules run in the sea level components step an output file containing these probability distributions. For application in the AR6, for example, the climate simulation was run offline and passed as an input to modules depending on these inputs.

2.3.2 Sea-level component modules

155 The bulk of the modules distributed with FACTS simulate physical processes that contribute to global-mean and/or relative sea level change.

Generic: The simplest module in FACTS 1.0 is the generic direct sampling module (`facts/directsample`), which simply translates an ensemble of time series samples specified in a text file into FACTS. For the implementation of FACTS to develop the IPCC Sixth Assessment Report sea-level projections, several of the modules used to simulate ice sheet and glacier

160 contributions (`ipccar6/ismipemuicesheets`, `ipccar6/gmipemuglaciers`, `ipccar6/larmipAIS`, `deconto21/AIS`, `bamber19/icesheets`) were based upon variants of `facts/directsample`, with the sample inputs being generated through offline simulation. (In the case of the first three modules, these offline simulations were driven by the same set of climate projections as used for other FACTS modules, with ordering and therefore climate-driven cross-model correlations preserved). For replicability reasons, the original AR6 direct-sample version of the emulandice ISMIP6 and LARMIP modules

165 (`ipccar6/ismipemuicesheets` and `ipccar6/larmipAIS`, respectively) are retained in FAIR 1.0, though their use is deprecated.

Greenland and Antarctic Ice sheets: In FACTS 1.0, the `larmip` and `emulandice` modules bring this formerly offline simulation within FACTS. These modules are both driven by sampled projections of global mean surface air temperature. The `emulandice` modules are structured as wrappers around separately developed, R-language Gaussian process emulators for

170 ISMIP6 ice sheet simulations and GlacierMIP glacier simulations, and demonstrates the ability of FACTS to incorporate independently developed models (Nowicki et al., 2016, 2020; Hock et al., 2019; Marzeion et al., 2020; Edwards et al., 2021). The ISMIP6 (Ice Sheet Model Intercomparison Project for CMIP6: Nowicki et al., 2016, 2020) project generated around 600 simulations from 2015-2100 from 27 modelling groups under very high (RCP8.5/SSP5-8.5) and low (RCP2.6/SSP1-2.6) emissions scenarios, systematically varying a small number of ice-sheet model parameters driving the response. These simulations

175 were used in constructing Gaussian Process emulators of the Greenland and Antarctic (West, East and Peninsula) contributions to sea level as a function of global mean surface air temperature and of these parameters (Edwards et al., 2021). Note that `emulandice` emulates sea level contributions in each year independently: the outputs are samples drawn from independent distributions for each year. This means it does not include temporal autocorrelation in uncertainty and therefore does not emulate the rates of change between years, although they can be approximated by smoothing the annual percentiles with a

180 temporal filter (temporal correlation emerges from the underlying simulations). Because the ISMIP6 experiments end in 2100, and Gaussian process emulation should not be used for significant extrapolation (being non-parametric), the `emulandice` modules cannot generate projections beyond 2100.

The `larmip` module is an adaptation of separately developed code, modified to achieve substantial speed improvements (Levermann et al., 2020). Within the Linear Antarctic Response Model Intercomparison Project (LARMIP-2), 16 state-of-the-

185 art ice-sheet models performed five experiments in which they switched on an additional basal ice shelf melting underneath five distinct regions of the Antarctic coast for 200 years. The time derivative of the ice loss response from these experiments yielded a linear response function for each of the regions in each of the models. These were convoluted with the basal melt

forcing from each of the global warming scenarios. These forcing time series were obtained from the scenario of the respected global mean temperature scenario, which was scaled and time-delayed in according with the response of the CMIP6 climate models' subsurface oceanic warming to a warming of the surface. This subsurface warming signal was then scaled with the observed interval of sensitivities of basal melting to warming outside of the Antarctic ice shelf cavities. In this way, a given global mean temperature scenario was translated into an ice-loss signal for each of the Antarctic regions.

Because the LARMIP-2 experiment examined only the dynamic response of the Antarctic ice sheet, projecting the full Antarctic response requires incorporating a separate term representing surface-mass balance changes. This is done using the same approach as in the `ipccar5/icesheets` modules, described below. Because the LARMIP-2 experiments end in 2100, projections are extrapolated beyond 2100 assuming a fixed rate of mass loss after 2100. This assumption probably yields an underestimate under higher emissions scenarios.

The `ipccar5/icesheets` module implements the Greenland and Antarctic ice sheet projection methods used in the IPCC Fifth Assessment Report (Church et al., 2013). Greenland surface mass balance is projected using a cubic polynomial of global mean surface air temperature (Fettweis et al., 2013). The polynomial is multiplied with a log-normally distributed factor representing methodological uncertainty. Another multiplier varying randomly between 1 and 1.15 is added to account for positive elevation feedback. For Antarctic surface mass balance, accumulation is projected to increase by $5.1 \pm 1.5\%$ per degree Celsius warming in Antarctica, with a 1.1 ± 0.2 ratio of warming in Antarctica to global mean surface air temperature increase. The uncertainties in both of these numbers are assumed to be normally distributed, and a negative rate is added to account for the feedback between enhanced accumulation and dynamic ice discharge. The ice dynamic contributions of Greenland and Antarctica are parameterized by quadratic functions of time, starting at either the lower or upper end of the uncertainty range of observed rates of ice loss over 2005-2010 and reaching respectively the minimum or maximum contributions of the ice sheets in 2100 that the Fifth Assessment Report assessed based on the available literature at that time. Samples are drawn assuming a uniform probability density in between these extreme quadratic functions (Church et al., 2013).

FACTS 1.0 also includes direct sampling modules used to incorporate ice-sheet projections that include, either by structured expert judgement (`bamber19/icesheets`) (Bamber et al., 2019) or physical modeling (`deconto21/AIS`) (DeConto et al., 2021), processes such as Marine Ice Cliff Instability that are not included in most ice-sheet models but that might have the potential to substantially accelerate the ice sheet contribution to sea level. Bamber et al. (2019) used formal structured expert judgement with calibrated expert responses to probabilistically evaluate Antarctic and Greenland mass loss through 2300 under 2°C and 5°C global temperature stabilization scenarios. In the IPCC AR6, these two temperature scenarios were applied in the context of integrated SSP1-2.6 and SSP5-8.5 projections. DeConto et al. (2021) projected future Antarctic ice sheet changes under the Representative Concentration Pathway (RCP) scenarios using a model that incorporates hydrofracturing of ice shelves and the gravitational instability of marine ice cliffs without the protection of a butressing ice shelf. In the IPCC AR6, the RCP scenario projections were appled in the context of the corresponding SSP projections (e.g., RCP2.6 projections from DeConto et al. (2021) applied to SSP1-2.6).

All the existing ice-sheet modules includes in their post-processing stage a regional scaling based on gravitational, rotational and deformational (GRD) fingerprints (Mitrovica et al., 2001). These fingerprints are implemented as static fingerprints that

do not change over time. They were pre-computed (outside the FACTS framework) by solving the sea-level equation with a
pseudo-spectral approach with a radially symmetric, elastic and compressible Earth model (Slangen et al., 2014).

225   *Glaciers:* The `emulandice/glacier` module, like the `emulandice/AIS` and `emulandice/GrIS` module, is based on
Gaussian process emulation of a multimodel intercomparison exercise, specifically the GlacierMIP2 ensemble (Marzeion et al.,
2020), and is driven by inputted global mean surface temperature trajectories. The GlacierMIP2 project generated nearly 300
simulations of 2015-2100 from 11 modelling groups under RCP scenarios. These simulations were used in constructing Gaus-
sian Process emulators of the 19 glacier region contributions to sea level as a function of global mean surface air temperature

230   (Edwards et al., 2021). Because the GlacierMIP experiments end in 2100 (as for the ice sheets), the emulandice modules cannot
generate projections beyond 2100.

The `ipccar5/glaciers` module is based on the the glacier projection approach used in the IPCC Fifth Assessment Report
(Church et al., 2013), which models the global mean sea-level change due to the melt of glaciers as $fI(t)^p$, where $I(t)$
is the time-integral of global mean surface temperature at time t, and f and p are parameters estimated from simulations

235   of a set of glacier models. The glacier models are equally weighted and systematic uncertainty in the glacier projections
is accounted for by Monte Carlo sampling, assuming a normal distribution with a time-dependent model-specific standard
deviation. For the glacier projections of the IPCC Sixth Assessment Report, these parameters were also derived from the
simulations of GlacierMIP and GlacierMIP2 and added as calibration options to the `ipccar5/glaciers` module (Hock et al.,
2019; Marzeion et al., 2020; Fox-Kemper et al., 2021). (In this manuscript, as in IPCC AR6, we focus on the GlacierMIP2

240   calibration of this module). As the IPCC AR5 model itself does not disaggregate the glacier contribution into separate regions,
this disaggregation is based upon the time-varying proportion of the contributions of different glaciers in the median projection
of Kopp et al. (2014).

As described in Kopp et al. (2014), the `kopp14/glaciers` module projects the contribution of 17 different glaciers and
ice cap regions for different RCPs by employing a multivariate t-distribution of ice mass change estimated from the model

245   simulations of (Marzeion et al., 2012) for different source regions.

As with the ice sheet modules, the glacier modules scale their output in the post-processing stage using offline-calculated
fingerprints. The lookup library includes separate fingerprints for seventeen different glacier regions, and thus the spatial pattern
associated with glaciers as a whole can change over time in response to the spatial distribution of glacier mass loss.

Sterodynamics: Several modules are included to project sterodynamic sea-level change, i.e., the sum of global mean ther-

250   mosteric sea-level rise and ocean dynamic sea-level change (Gregory et al., 2019). As described in Fox-Kemper et al. (2021),
the `tlm/sterodynamics` module does so by taking as input the emulated ocean heat content from the `fair/temperature`
module and pre-processed gridded simulations of CMIP6 models. Global mean thermosteric sea-level rise is projected by sam-
pling from a distribution of time-invariant global expansion coefficients derived from CMIP6 simulations (Fox-Kemper et al.,
2021) and multiplying the emulated ocean heat content by those coefficients. The CMIP6 simulations that were used for the

255   calibration of the expansion coefficients are shown in Table A1. The resulting global mean thermosteric sea-level rise is then
combined with ocean dynamic sea-level change and the inverse barometer effect using the gridded output of CMIP6 models
(see the right column of Table A1 for the models that were used in (Fox-Kemper et al., 2021)), based on the time-varying cor-

relation structure between global mean thermal expansion and ocean dynamic sea-level change in the multi-model ensemble. The `tlm/sterodynamics` module expects the CMIP6 input to be pre-processed (e.g., dedrifted and regridded) a priori.

260   The sterodynamic component is also provided by the `kopp2014/sterodynamics` module, which implements the methodology of Kopp et al. (2014). In this module, drift-corrected global mean thermal expansion is characterized for specific Representative Concentration Pathway scenarios using a t-distribution with the mean and covariance derived from the CMIP5 multi-model ensemble. As in `tlm/sterodynamics`, ocean dynamic sea-level change (including the inverse barometer effect) are then projected using the time-varying correlation structure between global mean thermal expansion and dynamic sea level

265   in the multi-model ensemble.

As described in Church et al. (2013), the `ipccar5/thermalexpansion` module projects global mean thermosteric sea-level rise, taking as input the time-dependent mean and standard deviation of the global mean thermosteric sea-level rise simulated by a multi-model ensemble. Samples are drawn from the mean and standard deviation assuming a normal distribution. The same method was applied by several studies and reports published in between the Fifth and Sixth Assessment Reports

270   of the IPCC (Palmer et al., 2018, 2020; Hermans et al., 2021).

Land water storage: Two modules provide the land water storage component of sea-level change. As described in Kopp et al. (2014), the first, `kopp14/landwaterstorage`, estimates this component based on the relationship between changes in land water storage and global population change, using United Nations population projections. Reservoir storage is assumed to follow a sigmoidal function of population change, calibrated based on Chao et al. (2008). The relationship between groundwater

275   depletion and population change is based on linear fits to estimates of Wada et al. (2012) and Konikow (2011). The model-based estimate of Pokhrel et al. (2012) were included for sensitivity analysis (Kopp et al., 2014).

The second module, `ssp/landwaterstorage`, follows the methods of Kopp et al. (2014), except for three aspects: (1) instead of using scenario-independent global population projections, population projections of the different SSPs were used (Samir and Lutz, 2017); (2) the groundwater depletion component was multiplied by 0.8 to account for only 80% of depleted

280   groundwater reaching the ocean (Wada et al., 2016); and (3) the capability to add a temporally linear adjustment for projected reservoir storage based on planned dam construction was addded (and applied in AR6 projections using the Hawley et al. (2020) projections for 2020-2040).

Vertical land motion and glacio-isostatic adjustment: Vertical land motion (as well as the sea-surface height contribution from glacio-isostatic adjustment [GIA]) are provided by `kopp2014/verticalandmotion` module. As described in Kopp

285   et al. (2014), this module estimates a constant trend at each spatial location, based upon a Gaussian Process spatio-temporal analysis of tide-gauges in the Permanent Service for Mean Sea Level database. This Gaussian Process analysis modifies an estimated rate of long-term trend derived from a single GIA model (ICE5G-VM2-90), treating this GIA model as a prior mean rate estimate whose misfits are statistically corrected. Sensitivity tests show this approach exhibits little sensitivity to the choice of initial GIA model.

290   The spatiotemporal model assumes observed RSL can be described as the sum of a uniform (and independently estimated) global component, a regionally-varying, autocorrelated non-linear component (with a decorrelation time scale of order 1-3 years), and a regionally-varying constant trend. The spatial and temporal correlation scales of the regional components are

separately tuned along different coastal segments. The constant trend is assumed to equal the long-term contribution from VLM (including the VLM term arising from GIA), as well as from the sea-surface height trend arising from GIA, and is propagated into the projection. An alternative VLM approach is demonstrated by the `NZInsarGPS/verticallandmotion` module, which takes a gridded data file describing rates of land motion inferred from interferometric synthetic aperture radar (InSAR) data.

2.3.3 Totaling module

The `facts/total` module handles the aggregation of sea level component probability distributions into probability distributions for total GMSL and RSL change. This module takes as an input a configuration file pointing to the output files that constitute different Workflows (see Section 2.4).

2.3.4 ESL module

The `extremesealevel/pointsoverthreshold` module, which is based on the methods of Oppenheimer et al. (2019a) and Frederikse et al. (2020), first derives declustered extreme sea levels from tide gauge data from the GESLA2 database (Woodworth et al., 2016) using a peak-over-threshold method with a user-defined threshold percentile. A Generalized Pareto Distribution is then fitted to the declustered extremes using maximum likelihood estimation. Annual means are removed prior to the fitting stage. The estimated parameters and their uncertainty are used to generate ESL return-period curves. Below the support of the Generalized Pareto Distribution, a Gumbel distribution between Mean Higher High Water and the extremes threshold is assumed to compute the return periods instead, following (Buchanan et al., 2016). In the projection stage, the module augments the return-period curves by projected RSL change to project how the expected frequency of ESL events of different magnitudes change as the baseline height of the events is increased (Frederikse et al., 2020).

2.4 Workflows

In this paper, we demonstrate FACTS' capabilities by implementing seven different Workflows (Table 2). The Workflows align with those implemented by IPCC AR6, with the substitution of the temperature-driven `emulandice` and `larmip` modules for the approach of direct-sampling offline calculated values used in AR6. The Workflows share a common set of modules used for projecting vertical land motion (`kopp14/verticallandmotion`), sterodynamic sea level (`tlm/sterodynamics`), and land water storage (`ssp/landwaterstorage`). They differ based on their handling of the cryospheric components (ice sheets and glaciers).

Workflows 1e and 2e employ Gaussian Process emulation of ice sheet and glacier intercomparison exercise outputs for Greenland and glaciers and, in the case of Workflow 1e, Antarctica (i.e., `emulandice` in Table 2). However, the Gaussian Process emulator of Edwards et al. (2021) models each time point independently, and thus does not estimate rates. Because `emulandice` uses a non-parametric (Gaussian process) model, where no functional form is assumed, rather than a parametric model, in which dependencies are asserted, Workflows using `emulandice` modules can only project up to the end of the

Table 1. Modules included in FACTS 1.0

Category	Module	Drivers
Climate	`fair/temperature`	emissions
Generic sea level component	`facts/directsample`	static
Glaciers	`emulandice/glaciers`	temperature
Glaciers	`kopp14/glaciers`	static by RCP scenario
Glaciers	`ipccar5/glaciers`	temperature
Glaciers	`ipccar6/gmipemuglaciers` (deprecated)	static by SSP scenario
Antarctic and Greenland Ice Sheets	`bamber19/icesheets`	static by warming level scenario
Antarctic and Greenland Ice Sheets	`ipccar5/icesheets`	temperature
Antarctic and Greenland Ice Sheets	`ipccar6/ismipemuicesheets` (deprecated)	static by SSP scenario
Antarctic and Greenland Ice Sheets	`kopp14/icesheets`	static by RCP scenario
Antarctic Ice Sheet	`deconto21/AIS`	static by RCP scenario
Antarctic Ice Sheet	`emulandice/AIS`	temperature
Antarctic Ice Sheet	`ipccar6/larmipAIS` (deprecated)	static by SSP scenario
Antarctic Ice Sheet	`larmip/AIS`	temperature
Greenland Ice Sheet	`emulandice/GrIS`	temperature
Greenland Ice Sheet	`FittedISMIP/GrIS`	temperature
Land Water Storage	`kopp14/landwaterstorage`	static
Land Water Storage	`ssp/landwaterstorage`	population
Sterodynamic Sea Level	`kopp14/sterodynamics`	static by RCP scenario
Sterodynamic Sea Level	`ipccar5/thermalexpansion`	static by RCP scenario
Sterodynamic Sea Level	`tlm/sterodynamics`	ocean heat content
Vertical land motion	`kopp14/verticallandmotion`	static
Vertical land motion	`NZInsarGPS/verticallandmotion`	static
Integration	`facts/total`	sea level components
Extreme sea level	`extremesealevel/pointsoverthreshold`	total relative sea level

original simulations (rather than extrapolate beyond them) and therefore end in 2100. Workflows 1f and 2f therefore substi-
325 tute alternative, parametric representations for GrIS and glaciers. Workflows 2e and 2f differ from Workflows 1e and 1f by
employing an alternative Antarctic ice sheet emulator, provided by the `larmip` module. These four Workflows together form
the basis of the *medium confidence* projections presented by AR6 (Fox-Kemper et al., 2021) Workflows 3e, 3f and 4, by con-
trast, take alternative approaches to ice sheet representation intended to capture processes not represented in most ice-sheet
models. Workflows 3e and 3f employs the `deconto21` projections for Antarctica, while Workflow 4 employs structured expert

Table 2. Workflows used in this paper and in IPCC AR6 (Fox-Kemper et al., 2021)

Workflow	GrIS	AIS	Glaciers	Land Water	Sterodynamic	VLM
1e	emulandice	emulandice	emulandice	ssp	tlm	kopp14
1f	FittedISMIP	ipccar5	ipccar5 (GMIP2)	ssp	tlm	kopp14
2e	emulandice	larmip	emulandice	ssp	tlm	kopp14
2f	FittedISMIP	larmip	ipccar5 (GMIP2)	ssp	tlm	kopp14
3e	emulandice	deconto21	emulandice	ssp	tlm	kopp14
3f	FittedISMIP	deconto21	ipccar5 (GMIP2)	ssp	tlm	kopp14
4	bamber19	bamber19	ipccar5 (GMIP2)	ssp	tlm	kopp14

330   judgement-based projections (`bamber19`) for both Greenland and Antarctic ice sheets. These three Workflows are combined with the *medium confidence* Workflows to form the basis of the broader AR6 *low confidence* projections.

3   Results

All results presented are based on 2000 pseudo-random Monte Carlo samples. To illustrate the application of FACTS, we focus on GMSL projections and on RSL and ESL projections at a single site, New York City.

335   3.1   Temperature projections

FACTS experiments begin with the estimation of the global mean surface temperature response to emissions forcing, as projected by the FAIR climate emulator. By construction, these projections are generally consistent with those of AR6 (Lee et al., 2021), with median warming in 2100 above 1850-1900 of 1.6 C in SSP1-2.6, 2.6 C in SSP2-4.5, and 4.7 C in SSP5-8.5 (Table 3). Note that SSP1-2.6 is aligned with the Paris Agreement goal of limiting warming to well-below 2 C, while SSP2-4.5 is

340   closer to projected emissions under current policy. SSP5-8.5 emissions represent a high-end trajectory that would require a reversion to fossil-fuel-intensive development (Riahi et al., 2022).

3.2   Global-mean contributions from sea-level components

In the sea-level component step, FACTS estimates the contributions to future GMSL and RSL rise from the cryosphere, land water storage, and sterodynamics. Some sea-level components modules take the FAIR-projected warming as an input, while

345   others rely upon pre-computed projections, in some cases indexed by SSP or RCP emissions scenario (Table 2).

    Projected median and 17th-83rd percentile global-mean sea level contributions are shown in Table 3 and Figure 2. The cryosphere as a whole (including glaciers and polar ice sheets) dominates median projections for 2100 under all emissions scenarios, but the relative contribution of polar ice sheets in particular varies substantially across modules. This is particularly the case under very high emissions (SSP5-8.5/RCP8.5), where one module (`deconto21`) projects the Antarctic contribution to

350   be the single largest term. For the polar ice sheet contributions, GMSL contributions projected by different modules are similar
until 2040 but begin to diverge beyond 2050, and this divergence is larger for higher emission scenarios (Figure 2). By contrast,
both glacier modules (`ipccar5` and `emulandice`) remain consistent throughout this century; this is to be expected, given that
both are calibrated to the same underlying GlacierMIP ensemble of glacier model projections (Marzeion et al., 2020).

3.3   Total global mean sea-level change projections

355   Total GMSL projections (Table 4, Figure 3) are generally in close agreement between Workflows using the `emulandice`
emulators of ISMIP6 and GlacierMIP projections (i.e., Workflows 1e, 2e, and 3e) and the corresponding Workflows that
substitute parametric emulators (i.e., Workflows 1f, 2f, and 3f) (Table 4). For example, under SSP2-4.5, total projections are
0.50 (0.42–0.60, 17th–83rd percentile range) m under Workflow 1e and 0.49 (0.40–0.59) cm under Workflow 1f; differences
are smaller for lower emissions scenarios and for other Workflow pairs, and higher for higher emissions. For the remainder
360   of this paper, we therefore focus primarily on Workflows 1f, 2f, 3f, and 4. The text discusses primarily SSP5-8.5, for which
different Workflows show the greatest distinctions. Figures highlight the difference between SSP1-2.6 and SSP5-8.5, as these
are the two scenarios they can be projected using all Workflows.

Substantial differences arise between Workflows based particularly on the choice of Antarctic module. Under SSP5-8.5,
median projections for 2100 differ by 14 cm between Workflow 1f (Antarctica calibrated as per IPCC AR5: 0.66 (0.55-0.78) m)
365   and Workflow 2f (Antarctica calibrated to LARMIP2: 0.80 (0.60-1.00) m), with the latter projections also exhibiting fatter tails.
This reflects the differences seen at the component level (Table 3, Figure 2). Larger differences are seen under higher emissions
scenarios with the two Workflows that AR6 employed to incorporate *low confidence* processes. Both Workflow 3f (Antarctic
ice sheet modeling MICI: 0.97 (0.81-1.17) m) and Workflow 4 (both Antarctica and Greenland based on structured expert
judgement: 1.00 (0.69-1.64) m) have median projections for SSP5-8.5 exceeding those of the *medium confidence* Workflows by
370   at least 17–20 cm. The median projections for Workflow 3e and 4 are closely aligned, but the structured expert judgment-based
projections (Workflow 4) span a larger range, reflecting primarily greater Greenland ice sheet uncertainty than in Workflow 3f.

Figure 4 shows the relative contribution of different components to total projection variance under different Workflows.
Consistent with the observations above, by the end of the century, total variance is generally dominated by polar ice sheet un-
certainty over the course of the century, particularly under Workflows 2f, 3f and 4. In addition, the variance plots for workflows
375   1f and 3f reveal a positive interaction term: i.e., the variance of GMSL projections is greater than the sum of the variances of
the individual components. This positive interaction term arises because thermal expansion, glacier loss, and (in the *medium
confidence* Workflows) polar ice sheet loss share a common dependence on global mean surface air temperature and thus are
positively correlated.

3.4   Relative and extreme sea-level projections at New York City

380   The differences between projected GMSL rise and projected RSL rise at New York City are consistent with past studies (e.g.,
Kopp et al., 2014) (Table 4; Figures 5, 6, 7). The median contribution and variance arising from the distant Antarctic is increased
due to GRD effects, which cause West Antarctic Ice Sheet loss to cause about 20% greater sea level rise at New York City than

Table 3. GMSL Component Projections for 2100

Component	Module	SSP1-2.6	SSP2-4.5	SSP5-8.5
GSAT (°C)	`fair/temperature`	1.63 (1.35–1.99)	2.61 (2.19–3.12)	4.66 (3.96–5.55)
Glaciers	`emulandice/glaciers`	0.09 (0.07–0.11)	0.12 (0.10–0.14)	0.18 (0.15–0.20)
Glaciers	`ipccar5/glaciers`	0.09 (0.06–0.13)	0.12 (0.08–0.16)	0.16 (0.11–0.22)
Glaciers	`kopp14/glaciers`	0.11 (0.08–0.14)	0.13 (0.09–0.16)	0.17 (0.13–0.21)
Antarctica	`bamber19/icesheets`	0.10 (-0.01–0.26)	—	0.20 (0.02–0.57)
Antarctica	`deconto21/AIS`	0.08 (0.06–0.11)	0.09 (0.07–0.11)	0.34 (0.19–0.53)
Antarctica	`emulandice/AIS`	0.08 (0.03–0.14)	0.08 (0.03–0.14)	0.08 (0.03–0.14)
Antarctica	`ipccar5/icesheets`	0.06 (-0.01–0.14)	0.05 (-0.02–0.13)	0.04 (-0.04–0.11)
Antarctica	`kopp14/icesheets`	0.06 (-0.05–0.16)	0.05 (-0.06–0.16)	0.04 (-0.08–0.14)
Antarctica	`larmip/AIS`	0.13 (0.05–0.26)	0.14 (0.05–0.29)	0.15 (0.05–0.34)
Greenland	`bamber19/icesheets`	0.13 (0.07–0.30)	—	0.22 (0.10–0.59)
Greenland	`emulandice/GrIS`	0.05 (0.01–0.10)	0.08 (0.04–0.13)	0.12 (0.08–0.18)
Greenland	`FittedISMIP/GrIS`	0.08 (0.06–0.10)	0.10 (0.08–0.12)	0.14 (0.11–0.18)
Greenland	`ipccar5/icesheets`	0.08 (0.05–0.10)	0.09 (0.07–0.13)	0.16 (0.11–0.22)
Greenland	`kopp14/icesheets`	0.06 (0.03–0.11)	0.08 (0.03–0.15)	0.14 (0.07–0.25)
Land Water Storage	`kopp14/landwaterstorage`	0.05 (0.03–0.07)	0.05 (0.03–0.07)	0.05 (0.03–0.07)
Land Water Storage	`ssp/landwaterstorage`	0.03 (0.02–0.04)	0.03 (0.02–0.04)	0.03 (0.02–0.04)
Thermal Expansion	`ipccar5/thermalexpansion`	0.15 (0.13–0.18)	0.21 (0.18–0.23)	0.32 (0.28–0.36)
Thermal Expansion	`tlm/sterodynamics`	0.14 (0.11–0.17)	0.19 (0.15–0.23)	0.29 (0.24–0.35)

Median (17th-83rd percentile) projections are shown relative to a 1995–2014 baseline. All are in m except for global mean surface air temperature (GSAT), which is in °C above a 1850–1900 baseline. For certain modules, projections for Representative Concentration Pathways 2.6, 4.5, and 8.5 are shown in lieu of those for the SSP scenarios.

in the global mean; while the median contributions and variance arising from the Greenland Ice Sheet and global glaciers are reduced due to relative proximity. The median sterodynamic contribution and its variance are larger than global mean thermal expansion due to the potential contribution from a slowdown of the Atlantic Meridional Overturning Circulation (Yin et al., 2009; Yin and Goddard, 2013). A long-term glacial isostatic adjustment trend, arising primarily from land subsidence, adds a steady 1.5 ± 0.2 mm/yr to RSL rise, shifting all projections upward but contributing little to variance.

As with GMSL projections, substantial differences arise between Workflows based particularly on the choice of Antarctic module. Under SSP5-8.5, Workflow 1f (0.90 [0.71–1.10] m) and Workflow 2f (1.07 [0.86–1.34] m) differ by 17 cm in the median. Further differences are seen with the two Workflows that AR6 employed to incorporate *low confidence* processes. Notably, because high-end GMSL projections in Workflow 4 include a larger Greenland contribution than in other Workflows, and because Greenland's effects on RSL rise at New York City are less than in GMSL rise, median Workflow 4 RSL projections

Table 4. Total Projections for 2100

Workflow	SSP1-1.9	SSP1-2.6	SSP2-4.5	SSP3-7.0	SSP5-8.5
Global mean sea level					
1e	0.35 (0.27–0.44)	0.40 (0.32–0.49)	0.50 (0.42–0.60)	0.62 (0.53–0.73)	0.71 (0.61–0.82)
1f	0.35 (0.27–0.44)	0.40 (0.31–0.49)	0.49 (0.40–0.59)	0.58 (0.48–0.68)	0.66 (0.55–0.78)
2e	0.40 (0.30–0.53)	0.46 (0.35–0.60)	0.57 (0.45–0.73)	0.70 (0.57–0.88)	0.80 (0.65–1.00)
2f	0.41 (0.33–0.54)	0.48 (0.38–0.62)	0.59 (0.48–0.74)	0.70 (0.58–0.87)	0.80 (0.66–1.00)
3e	—	0.40 (0.34–0.48)	0.51 (0.45–0.59)	—	0.97 (0.80–1.18)
3f	—	0.43 (0.37–0.49)	0.53 (0.47–0.61)	—	0.97 (0.81–1.17)
4	—	0.53 (0.37–0.80)	—	—	1.01 (0.69–1.64)
Relative sea level at New York City					
1e	0.56 (0.36–0.79)	0.62 (0.45–0.79)	0.75 (0.58–0.93)	0.86 (0.69–1.04)	0.97 (0.79–1.15)
1f	0.55 (0.33–0.77)	0.60 (0.42–0.78)	0.72 (0.54–0.90)	0.81 (0.62–0.99)	0.90 (0.71–1.10)
2e	0.64 (0.41–0.88)	0.70 (0.50–0.91)	0.85 (0.65–1.07)	0.97 (0.76–1.21)	1.09 (0.86–1.35)
2f	0.64 (0.41–0.89)	0.70 (0.51–0.92)	0.84 (0.65–1.07)	0.95 (0.74–1.19)	1.07 (0.86–1.34)
3e	—	0.63 (0.47–0.80)	0.77 (0.62–0.94)	—	1.27 (1.04–1.51)
3f	—	0.64 (0.48–0.81)	0.78 (0.62–0.94)	—	1.26 (1.03–1.51)
4	—	0.71 (0.48–0.97)	—	—	1.22 (0.89–1.73)

Median (17th-83rd percentile) projections are shown in meters relative to a 1995-2014 baseline.

(1.22 [0.88–1.73] m) are lower than Workflow 3e (1.27 [1.04–1.51] m), which relies more heavily on Antarctica to drive high-end GMSL rise. While the Workflow 4 tail remains the fattest of all Workflows, Workflow 3e's tail is fattened substantially as compared to GMSL because of the heightened response of New York City RSL to Antarctic mass loss.

Differences in RSL projections translate into differences in ESL projections (Table 5, Figure 8). For example, under Workflow 1f, the historic 1% average annual probability extreme sea level at New York City (estimated at 1.83 m above Mean Higher High Water) is projected to occur 2.6 (1.8–4.2) times more often by 2050 and 6.5 (3.2–17.2) times more often by 2100 under SSP1-2.6 due to the effects of RSL rise, and 2.8 (1.9–4.7) times more often by 2050 and 22.1 (8.0–90.3) times more often by 2100 under SSP5-8.5. 83rd percentile projected amplification factors are all < 6.8 by 2100 under SSP1-2.6, but under SSP5-8.5 and Workflow 4, the 83rd percentile SSP5-8.5 amplification factor exceeds 10,000 – meaning that, under the high end of this fat-tailed projection, the historic 100-year ESL event might occur over 100 times per year. (Note that ESL return periods do not translate directly into flooding or flood damages; see Rasmussen et al. (2022) for a critique of amplification factors as a metric.)
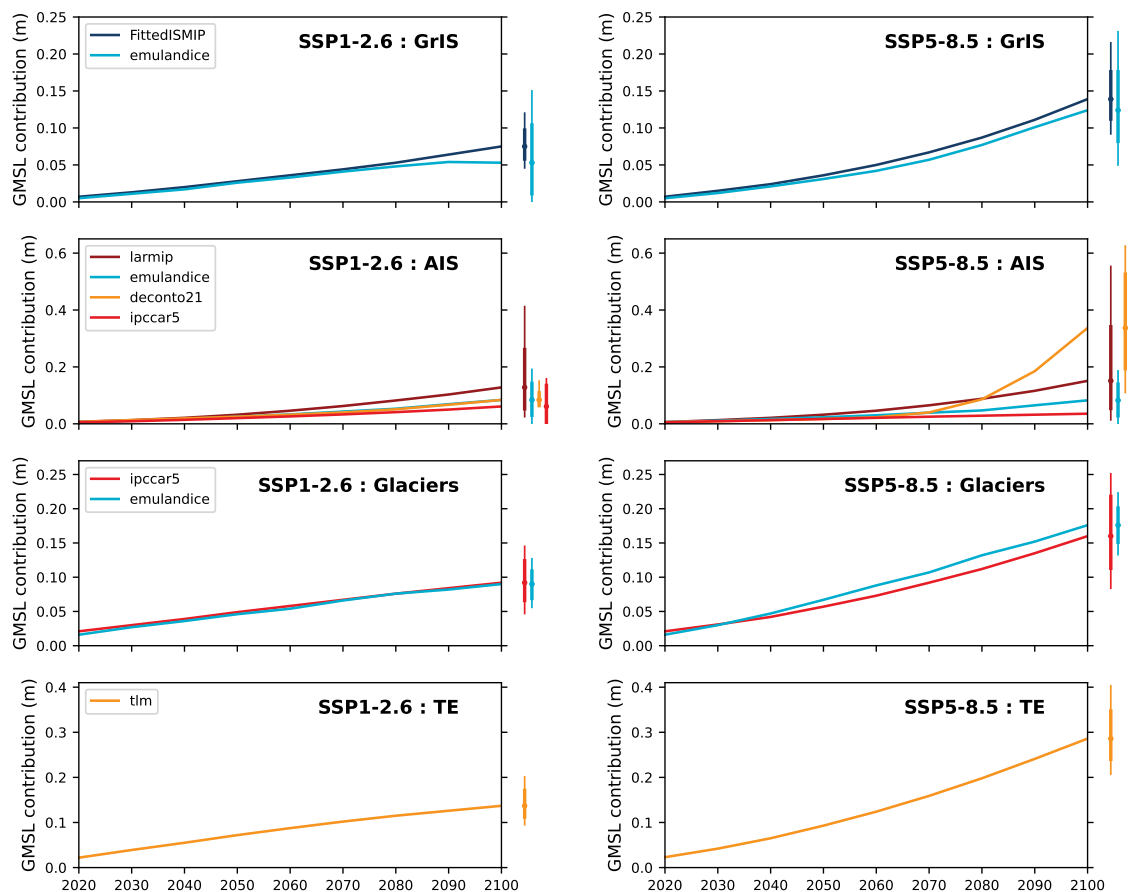
Figure 2. GMSL contributions from the Greenland ice sheet, the Antarctic ice sheet, glaciers, and thermal expansion for SSP1-2.6 and SSP5-8.5, based upon different FACTS modules. Curves show median projections. Thick/think bars at right show 17-83rd/5-95th percentile projections for 2100.

4 Discussion

4.1 Applications to date

The modular approach adopted by FACTS intentionally lends itself to careful consideration of both parametric and structural uncertainty in sea-level projections. Indeed, FACTS modules have already been used to support several major assessments of sea-level change. As previously noted, the IPCC AR6 sea-level projections were developed using FACTS modules, and the example Workflows described in this paper replicate the AR6 analysis.

AR6 followed the development of Workflow probability distributions with a particular approach to combined alternative probability distributions based upon probability boxes, or p-boxes (Kriegler and Held, 2005; Le Cozannet et al., 2017). P-boxes describing a set of probability distributions encompass the cumulative distribution functions of the underlying probabilities; for
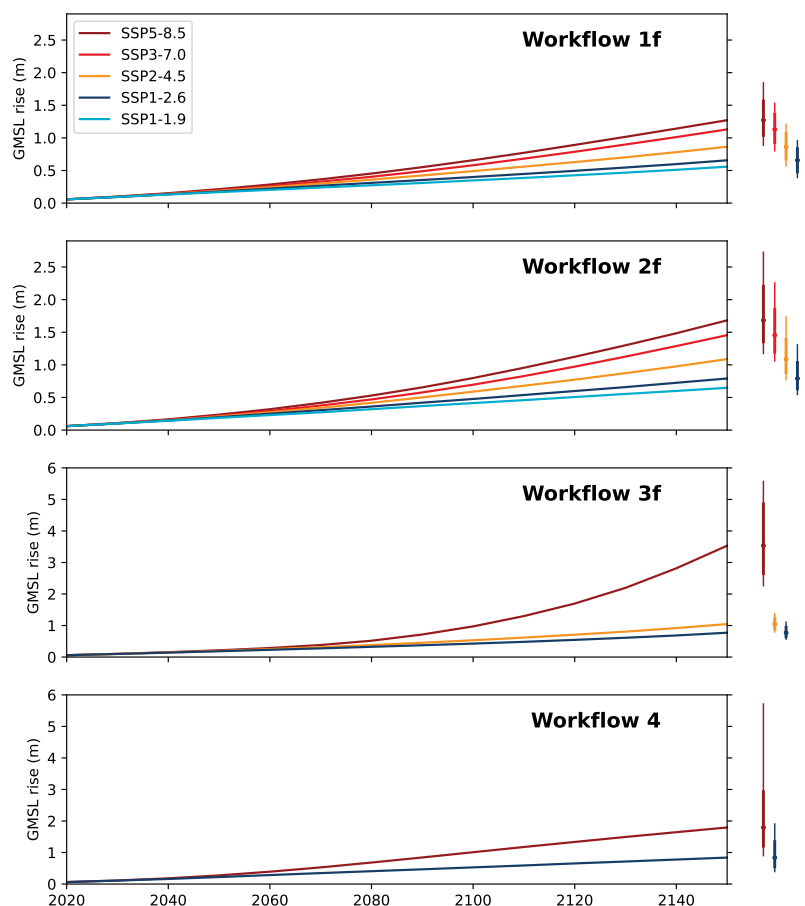
Figure 3. Total GMSL projections under four different Workflows under different SSP scenarios. Curves show median projections. Thick/-think bars at right show 17-83rd/5-95th percentile projections for 2150. Note change of y-axis scale between Workflows 1f and 2f (top two rows), representing *medium confidence* processes, and Workflows 3e and 4, which include *low confidence* processes.

example, the outer 17th-83rd percentile range of a p-box spans from the lowest 17th percentile of all distributions considered
415 to the highest 83rd-percentile. All the distributions considered by construction agree that there is *at least* a 66% chance that
the true value falls within this particular range. Fox-Kemper et al. (2021) used outer 17th–83rd percentile p-box ranges to
characterize its *likely* ranges, where *likely* in IPCC terminology means a 66–100% chance (Mastrandrea et al., 2010). (This is
a difference from the definition of *likely range* used in the rest of the IPCC AR6 WG1 report, which specifically refers to the
17th–83rd percentile of a single estimated probability distribution.) Workflows employing ISMIP and GlacierMIP emulators
420 (1e, 2e, and 3e) were preferred over those with simple parametric representations for land ice where possible, but Workflows
employing these simple representations (1f, 2f and 3f) were used when required for rates, which were not emulated. Workflows
1e/1f and 2e/2f were combined in a p-box to produce the AR6 *medium confidence* projections, while Workflows 3e/3f and 4
were added for *low confidence* projections.
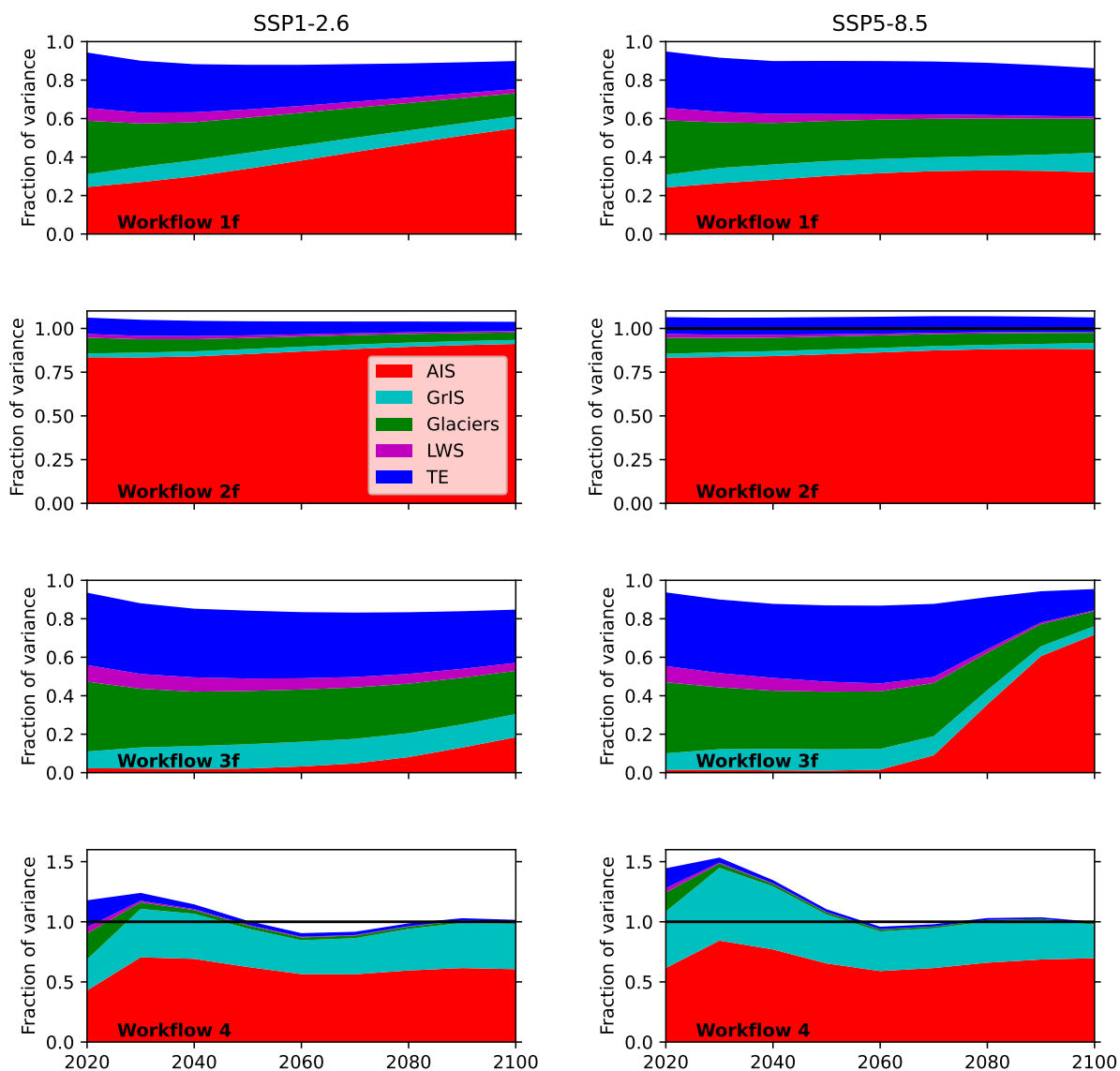
Figure 4. Variance decomposition of GMSL change in 2100 under SSP1-2.6 (left column) and SSP5-8.5 (right column), under Workflows 1f, 2f, 3f and 4. Colors correspond to different components. The difference between fraction of variance = 1.0 and the sum of the individual variances represents the interaction among components.

The US Interagency Task Force on sea-level rise Scenarios (Sweet et al., 2022) built upon the same FACTS output as AR6, but took a different approach to summarizing their results. Intending to produce a set of plausible global and regional sea-level scenarios to guide decision making – rather than, as in AR6, to characterize the likelihood of different future outcomes – the Task Force filtered the samples of sea-level rise associated with Workflows 1f, 2f, 3f and 4 to identify five subsets consistent
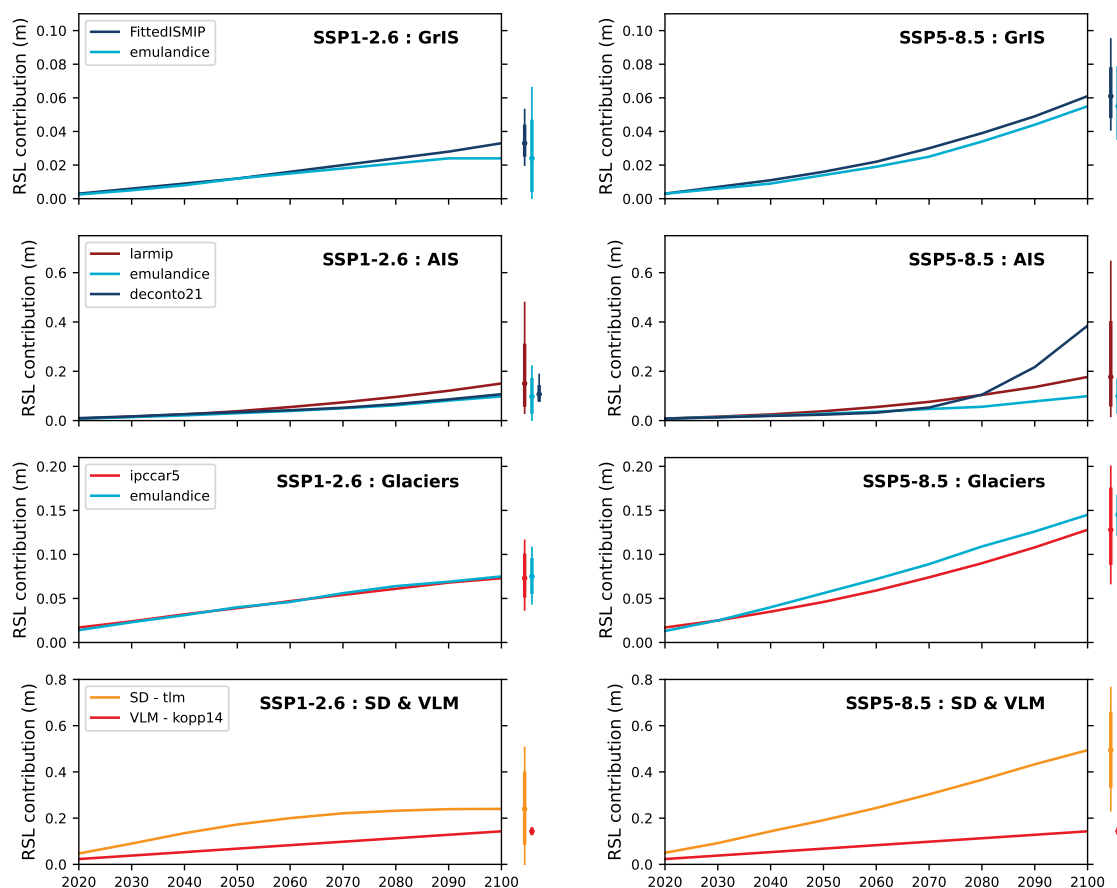
Figure 5. Projected New York City RSL contributions from the Greenland ice sheet, the Antarctic ice sheet, glaciers, and sterodynamic sea level from different FACTS modules under SSP1-2.6 and SSP5-8.5. Curves show median projections. Thick/think bars at right show 17-83rd/5-95th percentile projections for 2100.

with a range of 21st century GMSL rise. This range was semi-independently defined, based in part on an interpretation of the range of values presented in the AR6, to span from as low as 30 cm (roughly, a continuation of late 20th century GMSL range) to as high as 2.0 m, the latter informed by AR6's conclusion that low-likelihood, high-impact processes could elevate GMSL above the *likely* range by more than one metre. The median of each subset forms the center of each set of GMSL and RSL scenarios, while the 17th and 83rd percentiles of each subset provide within-scenario high/low sensitivity cases.

Both IPCC and the US Interagency Task Force invested significant effort in communicating these projections. For example, the NASA Sea Level Change Team, in partnership with these two groups, developed interactive projection viewers (at https://sealevel.nasa.gov/ipcc and https://sealevel.nasa.gov/task-force-scenario-tool) to allow practitioners to explore the projections for sites around the world and the US, respectively.
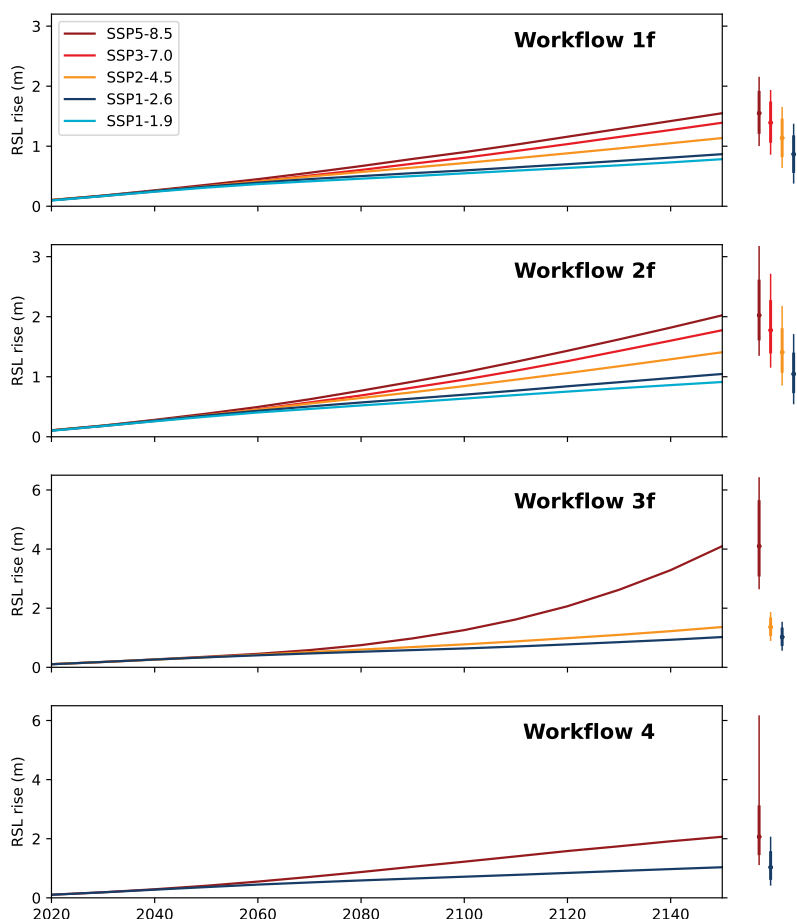
Figure 6. Total RSL projections for New York City under four different Workflows under different SSP scenarios. Curves show median projections. Thick/think bars at right show 17-83rd/5-95th percentile projections for 2150.

FACTS has also been used to develop national RSL projections for New Zealand (Levy et al., 2020; Naish et al., in review). In these studies, existing Workflows (either based on Kopp et al. (2014) or matching those employed in AR6) were amended by replacing the existing Kopp et al. (2014)-based projections of GIA and vertical land motion with gridded estimates based
440   on interferometric synthetic aperture radar (InSAR) data, calibrated with ground-based Global Navigation Satellite System (GNSS) measurements. This substitution reflects a need common to many national and subnational sea-level assessments, which seek consistency with broader assessments while substituting in information that can be assessed in greater detail at a local scale.

4.2   Directions for improvement

445   From a scientific perspective, a number of different directions promise improvement in FACTS projections.
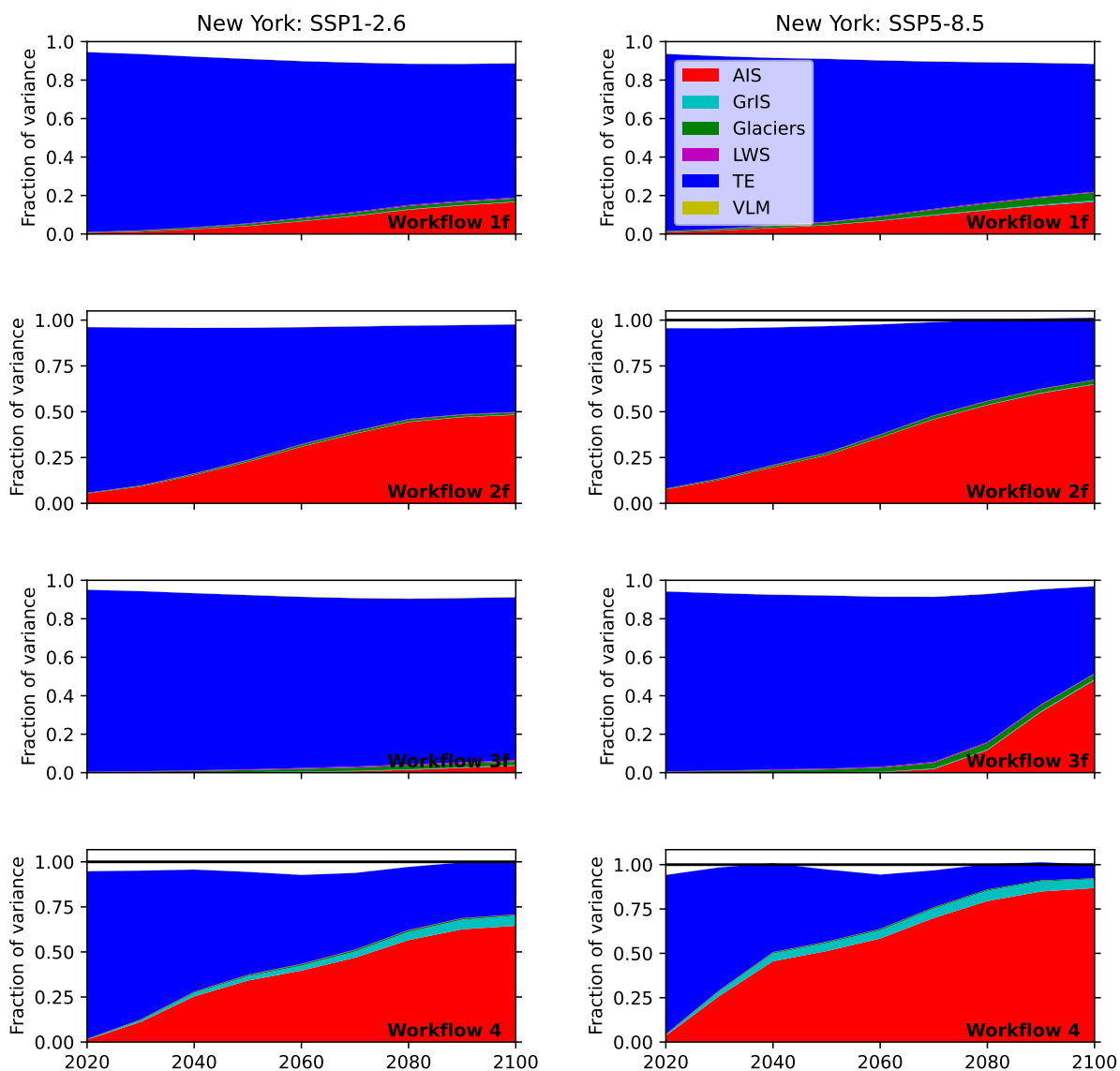
Figure 7. Variance decomposition of New York City RSL change in 2100 under SSP1-2.6 (left column) and SSP5-8.5 (right column), under Workflows 1f, 2f, 3f and 4.

At present, many but not all the modules within FACTS accept climate information as an input. In particular, the ice-sheet modules used to project deeply uncertain ice-sheet processes (the `bamber19/icesheets` and `deconto21/AIS` modules) rely upon direct sampling of output generated by individual studies (Bamber et al., 2019; DeConto et al., 2021). This means they can be applied only to a limited set of climate scenarios. For example, Bamber et al. (2019) produced projections for 2°C and 450 5°C temperature stabilization scenarios. With some caveats, these are used by AR6 to inform the projections for SSP1-2.6 and
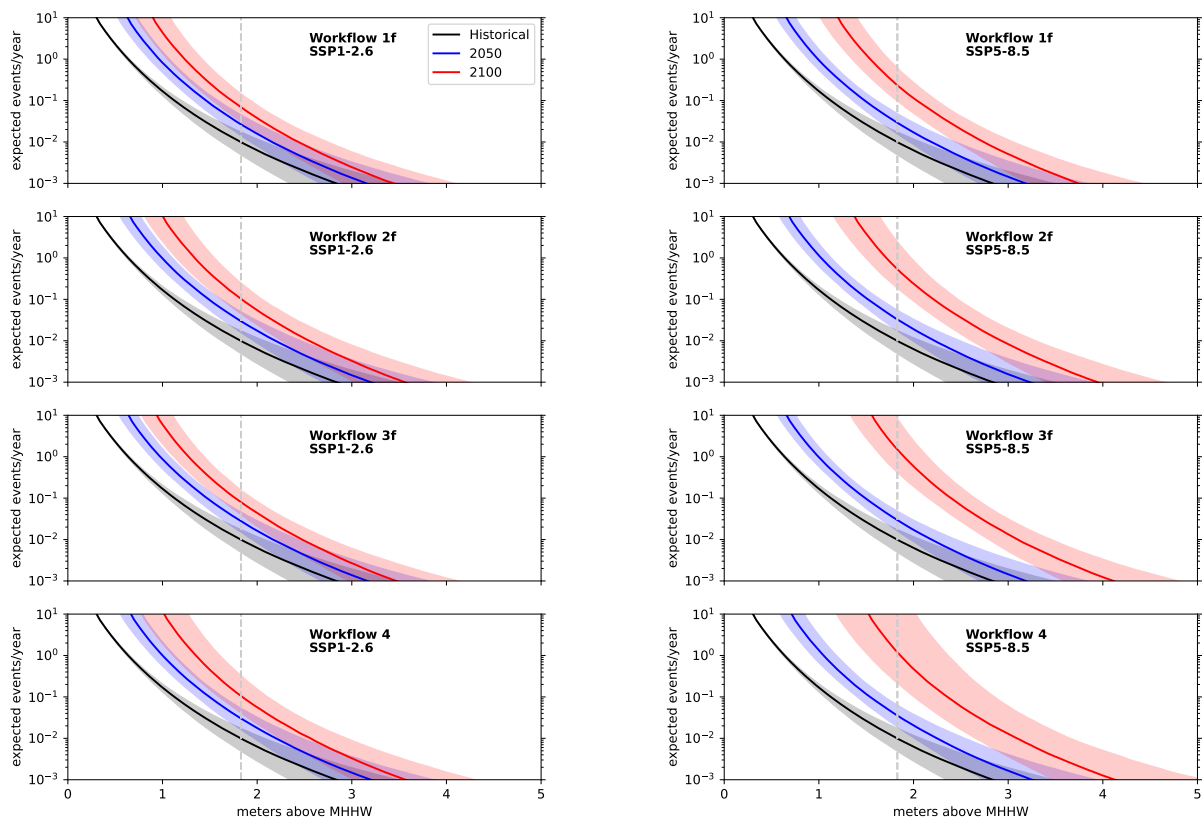
Figure 8. Extreme sea-level return-period curves at New York City under SSP1-2.6 and SSP5-8.5, under Workflows 1f, 2f, 3f and 4, in the historical period (black) and the years 2050 (blue) and 2100 (red). Solid line shows median projection; shading shows 17th-83rd percentile estimates. Dashed vertical line indicates the extreme sea-level height associated with the historic 1% average annual probability event.

Table 5. Frequency amplification factors in the years 2050 and 2100 for the historic 1% average annual probability (100-year return period) extreme sea-level event at New York City

Workflow	2050		2100	
	SSP1-2.6	SSP5-8.5	SSP1-2.6	SSP5-8.5
1f	2.6 (1.8–4.2)	2.8 (1.9–4.7)	6.5 (3.2–17.2)	22.1 (8.0–90.3)
2f	2.9 (1.9–4.8)	3.2 (2.1–5.4)	10.0 (4.1–33.8)	55.7 (13.0–451.2)
3f	2.7 (1.9–4.3)	2.9 (2.0–4.7)	7.6 (3.7–19.6)	146.5 (27.6–1629.2)
4	2.9 (1.9–5.2)	3.4 (2.1–6.8)	9.9 (4.0–43.6)	126.4 (16.3–10,283.4)

Median (17th-83rd percentile) projections are shown, as ratio of event probability in 2050 or 2100 to event probability in 1995–2014.

SSP5-8.5 (though SSP1-2.6 most likely stabilizes below 2°C and SSP5-8.5 continues after 2100 to warm well above 5°C). Generalizing emulation approaches to encompasses these alternative sources of information would allow projections of *low confidence* processes to be generated for arbitrary climate scenarios; doing this cautiously might require either advances in the primary literature or a great deal of humility and uncertainty regarding the assumptions used for scenario interpolation. (It is

455   difficult, for example, to infer the warming level associated with critical thresholds in ice sheet behavior from only two climate scenarios.)

The existing VLM modules assume a constant-rate trend into the future. While perhaps the best assumption that can be undertaken at a global scale, more refined approaches might be possible at a local scale. For example, in many regions, VLM is driven in part by highly-localised subsidence associated with anthropogenic interventions, such as fluid withdrawal and/or

460   surface loading (Shirzaei et al., 2021). Indeed, in the regions of the world experiencing the fastest rates of RSL rise, these currently tend to be the largest drivers. In such cases, assumption of a constant-rate trend in future may not be the most suitable assumption. A module capable of representing alternative scenarios of such factors could be helpful in assessments in such regions (e.g., Minderhoud et al., 2020). Alternatively, such scenarios might be independently added to RSL projections that have the VLM component removed.

465   The existing ESL module treats the shape and scale of ESL return period curves as stationary, with the distribution only shifted vertically by the increment of RSL change. In fact, ESL return periods will change due to processes such as shifts in tropical cyclone intensity and tracks (Fox-Kemper et al., 2021), and an enhanced ESL module could incorporate parametric representations of such changes. A further refinement could capture the relationship between these changes and global mean surface air temperature, allowing the analysis to reflect correlations between RSL change and storm changes (Lockwood et al.,

470   2022). Alternative ESL modules might also use different data sources, such as regional or global hydrodynamic models (e.g., Dullaart et al., 2020).

GRD processes in current FACTS modules are currently based on a library of scaling factors (sometimes called 'fingerprints') applied to ice sheet, glaciers, and land water storage projections in each module's post-processing step. Such a library approach is most appropriate for glaciers. For the larger ice sheets, however, the locus of ice mass change can significantly

475   affect the GRD spatial pattern (Larour et al., 2017; Mitrovica et al., 2018). This variability could be incorporated into FACTS by combining more spatially resolved ice sheet emulation with a new integration module that includes an online GRD solver (e.g., Larour et al., 2020).

The existing FACTS modules start projections in the year 2005, the centerpoint of the 1995-2014 historical baseline period used by AR6. This choice is, in part, a limitation of the underlying studies on which these modules are built. While CMIP6

480   historical climate simulations start in 1850, neither the GlacierMIP not ISMIP6 model intercomparison exercises include historical simulations (Nowicki et al., 2016, 2020; Hock et al., 2019; Marzeion et al., 2020). Implementing work-arounds to these absences – and incorporating new historical simulations as they become available – would allow FACTS projections to start in the 19th or 20th century, and thus enable model/data comparison for changes in both sea level and individual components. This, in turn, could allow the probability distributions generated FACTS to be updated in a Bayesian sense based

485   on historical, current, and (as time proceeds) future observations. While current observations are unlikely to significant reduce

the deep uncertainty associated with late-21st century high-end projections (Kopp et al., 2017), they could have a substantial impact on nearer-term projections. A Bayesian approach could also be coupled to economic models (e.g. Depsky et al., 2022) to assess the value of information associated with additional observational constraints and process-model enhancements.

Relevant to such model-data comparison is that the existing FACTS sea-level component modules are focused on project-490 ing changes in tidal-datum-epoch (i.e., 19-year) average mean sea level, not higher frequency (e.g., interannual) variability. Alternative ocean dynamics modules could introduce this higher frequency variability, or, alternatively, the auto-correlation structure of such variability could be incorporated into model/data comparisons.

Some modeling approaches may require greater communication between modules. At the moment, all sea-level components are computed independently, conditional upon a common input projections global mean surface air temperature and/or ocean 495 heat content in the climate step. As a consequence, uncertainty within individual Workflows is probably underestimated (e.g., Le Bars, 2018; van de Wal et al., 2022) While correlations between global mean surface air temperature and global ocean heat content change will tend to lead to some correlation between projected sea level components (e.g., Palmer et al., 2020), correlations associated with regional or systematic changes are not represented. This is not in the case in Earth system models, where (for example) meltwater input affects sterodynamic sea level (e.g., Lambert et al., 2021); representations of such interactions 500 could be incorporated into FACTS by subdividing the Sea Level Components Experiment Steps, either recursively refining projections with one-way coupling (e.g., modifying an initial dynamic sea-level projection for meltwater input) or proceeding in incremental time steps with two-way coupling.

More broadly, to date, FACTS has been developed by a small team, with a primary objective being to support specific assessment processes, particularly that of the IPCC AR6. A critical objective moving forward is to transform FACTS into 505 a larger-scale community project, with modules developed autonomously by different research and assessment teams. The structure of FACTS – which enables modules to serve as wrappers around independently developed code – is intended to facilitate such efforts.

5 Conclusions

Sea-level rise is a major driver of climate risk to coastal communities and ecosystems around the world. Appropriately manag-510 ing this risk requires planners to be cognizant of both quantifiable and structural uncertainty in projections of future sea-level change, and synthesizing this information is an important task of scientific assessment processes. FACTS provides a flexible, modular, and open-source platform that allows comparable probabilistic outputs to be generated in parallel through multiple modeling approaches. Its flexibility allows it to be customized based on the needs of specific assessment processes (e.g., substituting alternative approaches to VLM or higher-resolution sterodynamic sea level), while its parallel Workflow structure 515 supports the characterization of deep uncertainty.

Code availability. The development version of FACTS is available under a MIT license in a Git-version controlled repository at https://github.com/radical-collaboration/facts. The latest release is archived on Zenodo at https://doi.org/10.5281/zenodo.7502824. Documentation is included in the repository.

Data availability. Input data sets for the modules described in this manuscript are available on Zenodo at https://doi.org/10.5281/zenodo.7478191 and https://doi.org/10.5281/zenodo.7478447. Summary data sets describing the IPCC AR6 sea-level projections are available on Zenodo at https://doi.org/10.5281/zenodo.5914709.

Author contributions. REK, ABAS, and SJ conceived the project, and REK supervised and administered the project. GGG developed the FACTS architecture and most of the FACTS modules. REK, PK, TH, MT, AM, GK, and SJ contributed to code development. TLE (`emulandice`), REK (`kopp14`), AL (`larmip`), SN (`emulandice`), JG (`ipccar5`), MDP (`fair`) and CS (`fair`) led the initial development of individual module sets. All authors contributed to the writing and editing of the manuscript.

Competing interests. The authors declare that they have no conflict of interest.

Acknowledgements. GGG and REK were supported by grants from the National Science Foundation (ICER-1663807, ICER-2103754) and the National Aeronautics and Space Administration (grants 80NSSC17K0698, 80NSSC20K1724 and 80NSSC21K0322, and JPL task 105393.509496.02.08.13.31). REK was also supported by a grant from the Rhodium Group (for whom he has previously worked as a consultant) as part of the Climate Impact Lab consortium. This project was also supported by the U.K. Natural Environment Research Council (grants NE/T009381/1 and NE/T007443/1), by NIOZ Royal Netherlands Institute for Sea Research, by PROTECT, which has received funding from the European Union's Horizon 2020 research and innovation programme under grant agreement no. 869304, and by the NZ SeaRise Programme funded by New Zealand Ministry of Business, Innovation & Employment Contract to the Research Trust at Victoria University Contract ID - RTVU1705. MDP was supported by the Met Office Hadley Centre Climate Programme funded by BEIS. CS was supported by a NERC/IIASA collaborative research fellowship (NE/T009381/1).

We acknowledge the World Climate Research Programme, which, through its Working Group on Coupled Modelling, coordinated and promoted CMIP6. We thank the climate modeling groups for producing and making available their model output, the Earth System Grid Federation (ESGF) for archiving the data and providing access, and the multiple funding agencies who support CMIP6 and ESGF.

Table A1. CMIP6 models used for calibrating the thermal expansion coefficients of Fox-Kemper et al. (2021) (TE, left column) and for projecting ocean dynamic sea-level change and the inverse barometer effect (zos+psl, right column) in the `tlm/sterodynamics` module

Model	TE	zos+psl
ACCESS-CM2	x	x
ACCESS-ESM1-5	x	x
BCC-CSM2-MR		x
BCC-ESM1		x
CAMS-CSM1-0		x
CanESM5	x	x
CanESM5-CanOE		x
CAS-ESM2-0		x
CESM2		x
CESM2-FV2		x
CESM2-WACCM		x
CESM2-WACCM-FV2		x
CIESM		x
CMCC-CM2-SR5		x
CNRM-CM6-1	x	x
CNRM-CM6-1-HR	x	x
CNRM-ESM2-1	x	x
EC-Earth3	x	x
EC-Earth3-Veg	x	x
EC-Earth3-Veg-LR		x
FIO-ESM-2-0		x
GISS-E2-1-G		x
GISS-E2-1-G-CC		x
HadGEM3-GC31-LL	x	x
HadGEM3-GC31-MM		x
INM-CM4-8		x
INM-CM5-0	x	x
IPSL-CM6A-LR	x	x
MIROC6	x	x
MIROC-ES2L		x
MPI-ESM-1-2-HAM		x
MPI-ESM1-2-HR	x	x
MPI-ESM1-2-LR	x	x
MRI-ESM2-0	x	x
NorCPM1		x
NorESM2-LM	x	x
NorESM2-MM	x	x
UKESM1-0-LL	x	

References

540   Balasubramanian, V., Treikalis, A., Weidner, O., and Jha, S.: Ensemble Toolkit: Scalable and Flexible Execution of Ensembles of Tasks, in: 2016 45th International Conference on Parallel Processing (ICPP), pp. 458–463, https://doi.org/10.1109/ICPP.2016.59, 2016.

Balasubramanian, V., Turilli, M., Hu, W., Lefebvre, M., Lei, W., Modrak, R. T., Cervone, G., Tromp, J., and Jha, S.: Harnessing the Power of Many: Extensible Toolkit for Scalable Ensemble Applications, in: 2018 IEEE International Parallel and Distributed Processing Symposium, IPDPS 2018, Vancouver, BC, Canada, May 21-25, 2018, pp. 536–545, https://doi.org/10.1109/IPDPS.2018.00063, 2018.

545   Bamber, J. L., Oppenheimer, M., Kopp, R. E., Aspinall, W., and Cooke, R. M.: Ice sheet contributions to future sea level rise from structured expert judgement, Proceedings of the National Academy of Sciences, 116, 11 195–11 200, https://doi.org/10.1073/pnas.1817205116, 2019.

Buchanan, M. K., Kopp, R. E., Oppenheimer, M., and Tebaldi, C.: Allowances for evolving coastal flood risk under uncertain local sea-level rise, Climatic Change, 137, 347–362, https://doi.org/10.1007/s10584-016-1664-7, 2016.

550   Chao, B. F., Wu, Y. H., and Li, Y. S.: Impact of Artificial Reservoir Water Impound on Global Sea Level, Science, 320, 212–214, https://doi.org/10.1126/science.1154580, 2008.

Church, J. A., Clark, P. U., Cazenave, A., Gregory, J. M., Jevrejeva, S., Levermann, A., Merrifield, M. A., Milne, G. A., Nerem, R. S., Nunn, P. D., Payne, A. J., Pfeffer, W. T., Stammer, D., and Unnikrishnan, A. S.: Chapter 13: Sea Level Change, in: Climate Change 2013: the Physical Science Basis, edited by Stocker, T. F., Qin, D., Plattner, G.-K., Tignor, M., Allen, S. K., Boschung, J., Nauels, A., Xia, Y., Bex,
555   V., and Midgley, P. M., Intergovernmental Panel on Climate Change, http://www.ipcc.ch/report/ar5/wg1/, 2013.

DeConto, R. M., Pollard, D., Alley, R. B., Vellicogna, I., Gassons, E., Gomez, N., Rogstad, S., Gilford, D. M., Ashe, E. L., Kopp, R. E., Li, D., and Dutton, A. L.: The Paris Climate Agreement and future sea-level rise from Antarctica, Nature, 593, 83–88, https://doi.org/10.1038/s41586-021-03427-0, 2021.

Depsky, N., Bolliger, I., Allen, D., Choi, J. H., Delgado, M., Greenstone, M., Hamidi, A., Houser, T., Kopp, R., and Hsiang, S.: DSCIM-
560   Coastal v1.0: An Open-Source Modeling Platform for Global Impacts of Sea Level Rise, EGUsphere, https://doi.org/10.5194/egusphere-2022-198, 2022.

Dullaart, J., Muis, S., Bloemendaal, N., and Aerts, J. C.: Advancing global storm surge modelling using the new ERA5 climate reanalysis, Climate Dynamics, 54, 1007–1021, https://doi.org/10.1007/s00382-019-05044-0, 2020.

Edwards, T. L., Nowicki, S., Marzeion, B., Hock, R., Goelzer, H., Seroussi, H., Jourdain, N. C., Slater, D. A., Turner, F. E., Smith, C. J.,
565   McKenna, C. M., Simon, E., Abe-Ouchi, A., Gregory, J. M., Larour, E., Lipscomb, W. H., Payne, A. J., Shepherd, A., Agosta, C., Alexander, P., Albrecht, T., Anderson, B., Asay-Davis, X., Aschwanden, A., Barthel, A., Bliss, A., Calov, R., Chambers, C., Champollion, N., Choi, Y., Cullather, R., Cuzzone, J., Dumas, C., Felikson, D., Fettweis, X., Fujita, K., Galton-Fenzi, B. K., Gladstone, R., Golledge, N. R., Greve, R., Hattermann, T., Hoffman, M. J., Humbert, A., Huss, M., Huybrechts, P., Immerzeel, W., Kleiner, T., Kraaijenbrink, P., Le clec'h, S., Lee, V., Leguy, G. R., Little, C. M., Lowry, D. P., Malles, J.-H., Martin, D. F., Maussion, F., Morlighem, M., O'Neill, J. F.,
570   Nias, I., Pattyn, F., Pelle, T., Price, S. F., Quiquet, A., Radić, V., Reese, R., Rounce, D. R., Rückamp, M., Sakai, A., Shafer, C., Schlegel, N.-J., Shannon, S., Smith, R. S., Straneo, F., Sun, S., Tarasov, L., Trusel, L. D., Van Breedam, J., van de Wal, R., van den Broeke, M., Winkelmann, R., Zekollari, H., Zhao, C., Zhang, T., and Zwinger, T.: Projected Land Ice Contributions to Twenty-First-Century Sea Level Rise, Nature, 593, 74–82, https://doi.org/10.1038/s41586-021-03302-y, 2021.

Ellsberg, D.: Risk, ambiguity, and the Savage axioms, The Quarterly Journal of Economics, 75, 643–669, https://doi.org/10.2307/1884324,
575   1961.

Fettweis, X., Franco, B., Tedesco, M., Van Angelen, J., Lenaerts, J. T., van den Broeke, M. R., and Gallée, H.: Estimating the Greenland ice sheet surface mass balance contribution to future sea level rise using the regional atmospheric climate model MAR, The Cryosphere, 7, 469–489, https://doi.org/10.5194/tc-7-469-2013, 2013.

Fox-Kemper, B., Hewitt, H. T., Xiao, C., Aðalgeirsdóttir, G., Drijfhout, S. S., Edwards, T. L., Golledge, N. R., Hemer, M., Kopp, R. E., Krinner, G., Mix, A., Notz, D., Nowicki, S., Nurhati, I. S., Ruiz, L., Sallée, J.-B., Slangen, A. B. A., and Yu, Y.: Ocean, Cryosphere, and Sea Level Change, in: Climate Change 2021: The Physical Science Basis, edited by Masson-Delmotte, V., Zhai, P., Pirani, A., Connors, S. L., Péan, C., Berger, S., Caud, N., Chen, Y., Goldfarb, L., Gomis, M. I., Huang, M., Leitzell, K., Lonnoy, E., Matthews, J. B. R., Maycock, T. K., Waterfield, T., Yelekçi, O., Yu, R., and Zhou, B., pp. 1211–1362, Cambridge University Press, Cambridge, UK and New York, NY, USA, https://doi.org/10.1017/9781009157896.011, 2021.

Frederikse, T., Buchanan, M. K., Lambert, E., Kopp, R. E., Oppenheimer, M., Rasmussen, D., and van de Wal, R. S.: Antarctic Ice Sheet and emission scenario controls on 21st-century extreme sea-level changes, Nature communications, 11, 1–11, https://doi.org/10.1038/s41467-019-14049-6, 2020.

Garner, A. J., Weiss, J. L., Parris, A., Kopp, R. E., Horton, R. M., Overpeck, J. T., and Horton, B. P.: Evolution of 21st Century Sea-level Rise Projections, Earth's Future, 6, 1603–1615, https://doi.org/10.1029/2018EF000991, 2018.

Gornitz, V., Lebedeff, S., and Hansen, J.: Global sea level trend in the past century, Science, 215, 1611–1614, https://doi.org/10.1126/science.215.4540.1611, 1982.

Gregory, J., Griffies, S., Hughes, C., Lowe, J., Church, J., Fukumori, I., Gomez, N., Kopp, R., Landerer, F., Ponte, R., Stammer, D., Tamisiea, M., and van de Wal, R.: Concepts and terminology for sea level—mean, variability and change, both local and global, Surveys in Geophysics, https://doi.org/10.1007/s10712-019-09525-z, 2019.

Hall, J. A., Weaver, C. P., Obeysekera, J., Crowell, M., Horton, R. M., Kopp, R. E., Marburger, J., Marcy, D. C., Parris, A., Sweet, W. V., and Veatch, W. C.: Rising Sea Levels: Helping Decision-Makers Confront the Inevitable, Coastal Management, 47, 127–150, https://doi.org/10.1080/08920753.2019.1551012, 2019.

Hawley, W. B., Hay, C. C., Mitrovica, J. X., and Kopp, R. E.: A Spatially Variable Time Series of Sea Level Change due to Artificial Water Impoundment, Earth's Future, https://doi.org/10.1029/2020EF001497, 2020.

Hermans, T. H., Gregory, J. M., Palmer, M. D., Ringer, M. A., Katsman, C. A., and Slangen, A. B.: Projecting global mean sea-level change using CMIP6 models, Geophysical Research Letters, 48, e2020GL092 064, https://doi.org/10.1029/2020GL092064, 2021.

Hinkel, J., Church, J., Gregory, J., Lambert, E., Le Cozannet, G., Lowe, J., McInnes, K., Nicholls, R. J., Van der Pol, T., and van de Wal, R.: Meeting User Needs for Sea-Level Rise Information: A Decision Analysis Perspective, Earth's Future, 7, 320–337, https://doi.org/10.1029/2018EF001071, 2019.

Hock, R., Bliss, A., Marzeion, B., Giesen, R. H., Hirabayashi, Y., Huss, M., Radić, V., and Slangen, A. B. A.: GlacierMIP – A model intercomparison of global-scale glacier mass-balance models and projections, Journal of Glaciology, 65, 453–467, https://doi.org/10.1017/jog.2019.22, 2019.

Horton, B. P., Shennan, I., Bradley, S., Cahill, N., Kirwan, M., Kopp, R. E., and Shaw, T. A.: Predicting marsh vulnerability to sea-level rise using Holocene relative sea-level data, Nature Communications, 9, 2687, https://doi.org/10.1038/s41467-018-05080-0, 2018.

Jevrejeva, S., Frederikse, T., Kopp, R. E., Le Cozannet, G., Jackson, L. P., and van de Wal, R. S. W.: Probabilistic sea level projections at the coast by 2100, Surveys in Geophysics, 40, 1673–1696, https://doi.org/10.1007/s10712-019-09550-y, 2019.

Katsman, C. A., Church, J. A., Kopp, R. E., Kroon, D., Oppenheimer, M., Plag, H. P., Rahmstorf, S., Ridley, J., von Storch, H., and Vaughan, D. G.: High-End Projection for Local Sea Level Rise along the Dutch Coast in 2100 and 2200, Exploring high-end climate change scenarios for flood protection of the Netherlands. KNMI/Alterra, The Netherlands, pp. 15–81, 2008.

615 Konikow, L. F.: Contribution of global groundwater depletion since 1900 to sea-level rise, Geophysical Research Letters, 38, L17401, https://doi.org/10.1029/2011GL048604, 2011.

Kopp, R. E., Horton, R. M., Little, C. M., Mitrovica, J. X., Oppenheimer, M., Rasmussen, D. J., Strauss, B. H., and Tebaldi, C.: Probabilistic 21st and 22nd century sea-level projections at a global network of tide gauge sites, Earth's Future, 2, 383–406, https://doi.org/10.1002/2014EF000239, 2014.

620 Kopp, R. E., DeConto, R. M., Bader, D. A., Horton, R. M., Hay, C. C., Kulp, S., Oppenheimer, M., Pollard, D., and Strauss, B. H.: Evolving understanding of Antarctic ice-sheet physics and ambiguity in probabilistic sea-level projections, Earth's Future, 5, 1217–1233, https://doi.org/10.1002/2017EF000663, 2017.

Kopp, R. E., Gilmore, E. A., Little, C. M., Lorenzo Trueba, J., Ramenzoni, V. C., and Sweet, W. V.: Usable Science for Managing the Risks of Sea-Level Rise, Earth's Future, 7, 1235–1269, https://doi.org/10.1029/2018EF001145, 2019.

625 Kopp, R. E., Oppenheimer, M., O'Reilly, J. L., Drijfhout, S. S., Edwards, T., Fox-Kemper, B., Garner, G. G., Golledge, N. R., Hermans, T., Hewitt, H. T., Horton, B. P., Krinner, G., Notz, D., Nowicki, S., Palmer, M. D., and Slangen, A. B. A.: Communicating future sea-level rise uncertainty and ambiguity to assessment users, Nature Climate Change, https://doi.org/10.1002/essoar.10511663.1, in review.

Kriegler, E. and Held, H.: Utilizing belief functions for the estimation of future climate change, International journal of approximate reasoning, 39, 185–209, https://doi.org/10.1016/j.ijar.2004.10.005, 2005.

630 Lambert, E., Le Bars, D., Goelzer, H., and van de Wal, R. S.: Correlations Between Sea-Level Components Are Driven by Regional Climate Change, Earth's Future, 9, e2020EF001825, https://doi.org/https://doi.org/10.1029/2020EF001825, 2021.

Larour, E., Ivins, E. R., and Adhikari, S.: Should coastal planners have concern over where land ice is melting?, Science Advances, 3, e1700537, https://doi.org/10.1126/sciadv.1700537, 2017.

Larour, E., Caron, L., Morlighem, M., Adhikari, S., Frederikse, T., Schlegel, N.-J., Ivins, E., Hamlington, B., Kopp, R., and Nowicki, S.: 635 ISSM-SLPS: geodetically compliant Sea-Level Projection System for the Ice-sheet and Sea-level System Model v4.17, Geoscientific Model Development, 13, 4925–4941, https://doi.org/10.5194/gmd-13-4925-2020, 2020.

Le Bars, D.: Uncertainty in Sea Level Rise Projections Due to the Dependence Between Contributors, Earth's Future, 6, 1275–1291, https://doi.org/https://doi.org/10.1029/2018EF000849, 2018.

Le Cozannet, G., Manceau, J.-C., and Rohmer, J.: Bounding probabilistic sea-level projections within the framework of the possibility theory, 640 Environmental Research Letters, 12, 014012, https://doi.org/10.1088/1748-9326/aa5528, 2017.

Lee, J. Y., Marotzke, J., Bala, C., Cao, L., Corti, S., Dunne, J. P., Engelbrecht, F., Fischer, E., Fyfe, J. C., Jones, C., Maycock, A., Mutemi, J., Ndiaye, O., Panickal, S., and Zhou, T.: Future Global Climate: Scenario-Based Projections and near-Term Information, in: Climate Change 2021: The Physical Science Basis, edited by Masson-Delmotte, V., Zhai, P., Pirani, A., Connors, S. L., Péan, C., Berger, S., Caud, N., Chen, Y., Goldfarb, L., Gomis, M. I., Huang, M., Leitzell, K., Lonnoy, E., Matthews, J. B. R., Maycock, T. K., Water-645 field, T., Yelekçi, O., Yu, R., and Zhou, B., pp. 553–672, Cambridge University Press, Cambridge, UK and New York, NY, USA, https://doi.org/10.1017/9781009157896.011, 2021.

Lempert, R., Popper, S., and Bankes, S.: Shaping the next one hundred years: New methods for quantitative, long-term policy analysis, RAND Corporation, Santa Monica, California, 2003.

Levermann, A., Winkelmann, R., Albrecht, T., Goelzer, H., Golledge, N. R., Greve, R., Huybrechts, P., Jordan, J., Leguy, G., Martin, D.,
650   Morlighem, M., Pattyn, F., Pollard, D., Quiquet, A., Rodehacke, C., Seroussi, H., Sutter, J., Zhang, T., Van Breedam, J., Calov, R.,
       DeConto, R., Dumas, C., Garbe, J., Gudmundsson, G. H., Hoffman, M. J., Humbert, A., Kleiner, T., Lipscomb, W. H., Meinshausen, M.,
       Ng, E., Nowicki, S. M. J., Perego, M., Price, S. F., Saito, F., Schlegel, N.-J., Sun, S., and van de Wal, R. S. W.: Projecting Antarctica's
       Contribution to Future Sea Level Rise from Basal Ice Shelf Melt Using Linear Response Functions of 16 Ice Sheet Models (LARMIP-2),
       Earth System Dynamics, 11, 35–76, https://doi.org/10.5194/esd-11-35-2020, 2020.
655 Levy, R., Naish, T., Bell, R., Golledge, N., Clarke, L., Garner, G., Hamling, I., Heine, Z., Hreinsdottir, S., Lawrence, J., et al.: Te tai pari o
       Aotearoa–Future sea level rise around New Zealand's dynamic coastline, Coastal systems and sea level rise: What to look for in future.
       Special Publication, 4, 11–20, 2020.
     Lockwood, J. W., Oppenheimer, M., Lin, N., Kopp, R. E., Vecchi, G. A., and Gori, A.: Correlation Between Sea-Level Rise and Aspects of
       Future Tropical Cyclone Activity in CMIP6 Models, Earth's Future, 10, e2021EF002 462, https://doi.org/10.1029/2021EF002462, 2022.
660 Marzeion, B., Jarosch, A. H., and Hofer, M.: Past and future sea-level change from the surface mass balance of glaciers, The Cryosphere, 6,
       1295–1322, https://doi.org/10.5194/tc-6-1295-2012, 2012.
     Marzeion, B., Hock, R., Anderson, B., Bliss, A., Champollion, N., Fujita, K., Huss, M., Immerzeel, W. W., Kraaijenbrink, P., Malles, J.-H.,
       Maussion, F., Radić, V., Rounce, D. R., Sakai, A., Shannon, S., van de Wal, R., and Zekollari, H.: Partitioning the Uncertainty of Ensemble
       Projections of Global Glacier Mass Change, Earth's Future, 8, e2019EF001 470, https://doi.org/https://doi.org/10.1029/2019EF001470,
665   e2019EF001470 10.1029/2019EF001470, 2020.
     Mastrandrea, M. D., Field, C. B., Stocker, T. F., Edenhofer, O., Ebi, K. L., Frame, D. J., Held, H., Kriegler, E., Mach, K. J., and Matschoss,
       P. R.: Guidance note for lead authors of the IPCC fifth assessment report on consistent treatment of uncertainties, Intergovernmental Panel
       on Climate Change (IPCC), 2010.
     Meehl, G., Stocker, T., Collins, W., Friedlingstein, P., Gaye, A., Gregory, J., Kitoh, A., Knutti, R., Murphy, J., Noda, A., et al.: Global climate
670   projections, in: Climate Change 2007: The Physical Science Basis: Fourth Assessment Report of the Intergovernmental Panel on Climate
       Change, edited by Solomon, S. et al., Cambridge University Press, Cambridge, UK, 2007.
     Mercer, J. H.: West Antarctic ice sheet and CO_2 greenhouse effect: a threat of disaster, Nature, 271, 321–325,
       https://doi.org/10.1038/271321a0, 1978.
     Merzky, A., Weidner, O., and Jha, S.: SAGA: A Standardized Access Layer to Heterogeneous Distributed Computing Infrastructure,
675   Software-X, https://doi.org/10.1016/j.softx.2015.03.001, 2015.
     Merzky, A., Turilli, M., Titov, M., Al-Saadi, A., and Jha, S.: Design and performance characterization of radical-pilot on leadership-class
       platforms, IEEE Transactions on Parallel and Distributed Systems, 33, 818–829, https://doi.org/10.1109/TPDS.2021.3105994, 2021.
     Millar, R. J., Nicholls, Z. R., Friedlingstein, P., and Allen, M. R.: A modified impulse-response representation of the global near-surface air
       temperature and atmospheric concentration response to carbon dioxide emissions, Atmospheric Chemistry and Physics, 17, 7213–7228,
680   https://doi.org/10.5194/acp-17-7213-2017, 2017.
     Minderhoud, P., Middelkoop, H., Erkens, G., and Stouthamer, E.: Groundwater extraction may drown mega-delta: projections of extraction-
       induced subsidence and elevation of the Mekong delta for the 21st century, Environmental Research Communications, 2, 011 005,
       https://doi.org/10.1088/2515-7620/ab5e21, 2020.
     Mitrovica, J. X., Tamisiea, M. E., Davis, J. L., and Milne, G. A.: Recent mass balance of polar ice sheets inferred from patterns of global
685   sea-level change, Nature, 409, 1026–1029, https://doi.org/10.1038/35059054, 2001.

Mitrovica, J. X., Gomez, N., and Clark, P. U.: The Sea-Level Fingerprint of West Antarctic Collapse, Science, 323, 753–753, https://doi.org/10.1126/science.1166510, 2009.

Mitrovica, J. X., Hay, C. C., Kopp, R. E., Harig, C., and Latychev, K.: Quantifying the Sensitivity of Sea Level Change in Coastal Localities to the Geometry of Polar Ice Mass Flux, Journal of Climate, 31, 3701–3709, https://doi.org/10.1175/JCLI-D-17-0465.1, 2018.

Muntjewerf, L., Sacks, W. J., Lofverstrom, M., Fyke, J., Lipscomb, W. H., Ernani da Silva, C., Vizcaino, M., Thayer-Calder, K., Lenaerts, J. T., and Sellevold, R.: Description and Demonstration of the Coupled Community Earth System Model v2–Community Ice Sheet Model v2 (CESM2-CISM2), Journal of Advances in Modeling Earth Systems, 13, e2020MS002 356, https://doi.org/10.1029/2020MS002356, 2021.

Naish, T., Levy, R., Hamling, I., Garner, G., Hreinsdóttir, S., Kopp, R., Golledge, N., King, N., Newnham, R., and Wallace, L.: The significance of vertical land movements at convergent plate boundaries in probabilistic sea-level projections for AR6 scenarios: The New Zealand case., Earth's Future, https://doi.org/10.1002/essoar.10511878.1, in review.

National Research Council: Responding to Changes in Sea Level: Engineering Implications, National Academies Press, 1987.

National Research Council: Sea-Level Rise for the Coasts of California, Oregon, and Washington: Past, Present, and Future, The National Academies Press, Washington, D.C., 2012.

Nowicki, S., Goelzer, H., Seroussi, H., Payne, A. J., Lipscomb, W. H., Abe-Ouchi, A., Agosta, C., Alexander, P., Asay-Davis, X. S., Barthel, A., Bracegirdle, T. J., Cullather, R., Felikson, D., Fettweis, X., Gregory, J. M., Hattermann, T., Jourdain, N. C., Kuipers Munneke, P., Larour, E., Little, C. M., Morlighem, M., Nias, I., Shepherd, A., Simon, E., Slater, D., Smith, R. S., Straneo, F., Trusel, L. D., van den Broeke, M. R., and van de Wal, R.: Experimental protocol for sea level projections from ISMIP6 stand-alone ice sheet models, The Cryosphere, 14, 2331–2368, https://doi.org/10.5194/tc-14-2331-2020, 2020.

Nowicki, S. M. J., Payne, A., Larour, E., Seroussi, H., Goelzer, H., Lipscomb, W., Gregory, J., Abe-Ouchi, A., and Shepherd, A.: Ice Sheet Model Intercomparison Project (ISMIP6) contribution to CMIP6, Geoscientific Model Development, 9, 4521–4545, https://doi.org/10.5194/gmd-9-4521-2016, 2016.

Oppenheimer, M., Glavovic, B., Hinkel, J., van de Wal, R., Magnan, A. K., Abd-Elgawad, A., Cai, R., Cifuentes-Jara, M., Deconto, R. M., Ghosh, T., Hay, J., Isla, F., Marzeion, B., Meyssignac, B., and Sebesvari, Z.: Sea Level Rise and Implications for Low Lying Islands, Coasts and Communities, in: IPCC Special Report on the Ocean and Cryosphere in a Changing Climate, edited by Pörtner, H.-O., Roberts, D. C., Masson-Delmotte, V., Zhai, P., Tignor, M., Poloczanska, E., Mintenbeck, K., Alegréia, A., Nicolai, M., Okem, A., Petzold, J., Rama, B., and Weyer, N. M., pp. 321–445, Cambridge University Press, Cambridge, UK and New York, NY, USA, 2019a.

Oppenheimer, M., Oreskes, N., Jamieson, D., Brysse, K., O'Reilly, J., Shindell, M., and Wazeck, M.: Discerning Experts: The Practices of Scientific Assessment for Environmental Policy, University of Chicago Press, Chicago, IL, 2019b.

Palmer, M., Gregory, J. M., Bagge, M., Calvert, D., Hagedoorn, J., Howard, T., Klemann, V., Lowe, J., Roberts, C., Slangen, A., et al.: Exploring the drivers of global and local sea-level change over the 21st century and beyond, Earth's Future, 8, e2019EF001 413, https://doi.org/10.1029/2019EF001413, 2020.

Palmer, M. D., Harris, G. R., and Gregory, J. M.: Extending CMIP5 projections of global mean temperature change and sea level rise due to thermal expansion using a physically-based emulator, Environmental Research Letters, 13, 084 003, https://doi.org/10.1088/1748-9326/aad2e4, 2018.

Pokhrel, Y. N., Hanasaki, N., Yeh, P. J.-F., Yamada, T. J., Kanae, S., and Oki, T.: Model estimates of sea-level change due to anthropogenic impacts on terrestrial water storage, Nature Geoscience, https://doi.org/10.1038/ngeo1476, 2012.

Rasmussen, D. J., Kulp, S., Kopp, R. E., Oppenheimer, M., and Strauss, B. H.: Popular extreme sea level metrics can better communicate impacts, Climatic Change, 170, 30, https://doi.org/10.1007/s10584-021-03288-6, 2022.

725 Riahi, K., Schaeffer, R., Arango, J., Calvin, K., Guivarch, C., Hasegawa, T., Jiang, K., Kriegler, E., Matthews, R., Peters, G., Rao, A., Robertson, S., Sebbit, A. M., Steinberger, J., Tavoni, M., and van Vuuren, D.: Mitigation Pathways Compatible with Long-Term Goals, in: Climate Change 2022: Mitigation of Climate Change, edited by Shukla, P. R., Skea, J., Reisinger, A., Slade, R., Fradera, R., Pathak, M., Al Kourdajie, A., Beklacemi, M., van Diemen, R., Hasija, A., Lisboa, G., Luz, S., Malley, J., McCollum, D., Some, S., and Vyas, P., vol. in press, Cambridge University Press, Cambridge, UK and New York, NY, USA, 2022.

730 Samir, K. and Lutz, W.: The human core of the shared socioeconomic pathways: Population scenarios by age, sex and level of education for all countries to 2100, Global Environmental Change, 42, 181–192, https://doi.org/10.1016/j.gloenvcha.2014.06.004, 2017.

Shirzaei, M., Freymueller, J., Törnqvist, T. E., Galloway, D. L., Dura, T., and Minderhoud, P. S.: Measuring, modelling and projecting coastal land subsidence, Nature Reviews Earth & Environment, 2, 40–58, https://doi.org/10.1038/s43017-020-00115-x, 2021.

Slangen, A., Carson, M., Katsman, C., Van de Wal, R., Köhl, A., Vermeersen, L., and Stammer, D.: Projecting twenty-first century regional
735 sea-level changes, Climatic Change, 124, 317–332, https://doi.org/10.1007/s10584-014-1080-9, 2014.

Slangen, A. B., Palmer, M. D., Camargo, C. M., Church, J. A., Edwards, T. L., Hermans, T. H., Hewitt, H., Garner, G. G., Gregory, J. M., Kopp, R. E., et al.: The evolution of 21st century sea-level projections from IPCC AR5 to AR6 and beyond, Cambridge Prisms: Coastal Futures, pp. 1–33, https://doi.org/10.1017/cft.2022.8, in press.

Smith, C. J., Forster, P. M., Allen, M., Leach, N., Millar, R. J., Passerello, G. A., and Regayre, L. A.: FAIR v1. 3: a simple emissions-based
740 impulse response and carbon cycle model, Geoscientific Model Development, 11, 2273–2297, https://doi.org/10.5194/gmd-11-2273-2018, 2018.

Smith, R. S., Mathiot, P., Siahaan, A., Lee, V., Cornford, S. L., Gregory, J. M., Payne, A. J., Jenkins, A., Holland, P. R., Ridley, J. K., et al.: Coupling the UK Earth System Model to dynamic models of the Greenland and Antarctic ice sheets, Journal of Advances in Modeling Earth Systems, 13, e2021MS002 520, https://doi.org/10.1029/2021MS002520, 2021.

745 Sweet, W. V., Hamlington, B. D., Kopp, R. E., Weaver, C. P., Barnard, P. L., Bekaert, D., W. Brooks, M. C., Dusek, G., Frederikse, T., Garner, G., Genz, A., Krasting, J. P., Larour, E., D. Marcy, J. J. M., Obeysekera, J., Osler, M., Pendleton, M., Roman, D., Schmied, L., Veatch, W., White, K. D., and Zuzak, C.: Global and Regional Sea Level Rise Scenarios for the United States: Updated Mean Projections and Extreme Water Level Probabilities Along U.S. Coastlines, NOAA Technical Report NOS 01, National Oceanic and Atmospheric Administration, National Ocean Service, Silver Spring, MD, https://oceanservice.noaa.gov/hazards/sealevelrise/
750 noaa-nos-techrpt01-global-regional-SLR-scenarios-US.pdf, 2022.

Turilli, M., Balasubramanian, V., Merzky, A., Paraskevakos, I., and Jha, S.: Middleware building blocks for workflow systems, Computing in Science & Engineering, 21, 62–75, https://doi.org/10.1109/MCSE.2019.2920048, 2019.

US Army Corps of Engineers: Letter on relative sea level change dated 21 March 1986, Tech. rep., USACE Directorate of Civil Works, Washington, DC, 1986.

755 van de Wal, R. S. W., Nicholls, R. J., Behar, D., McInnes, K., Stammer, D., Lowe, J. A., Church, J. A., DeConto, R., Fettweis, X., Goelzer, H., Haasnoot, M., Haigh, I. D., Hinkel, J., Horton, B. P., James, T. S., Jenkins, A., LeCozannet, G., Levermann, A., Lipscomb, W. H., Marzeion, B., Pattyn, F., Payne, A. J., Pfeffer, W. T., Price, S. F., Seroussi, H., Sun, S., Veatch, W., and White, K.: A High-End Estimate of Sea Level Rise for Practitioners, Earth's Future, 10, e2022EF002 751, https://doi.org/10.1029/2022EF002751, 2022.

Wada, Y., van Beek, L. P. H., Sperna Weiland, F. C., Chao, B. F., Wu, Y.-H., and Bierkens, M. F. P.: Past and future contribution of global
760 groundwater depletion to sea-level rise, Geophysical Research Letters, 39, L09 402, https://doi.org/10.1029/2012GL051230, 2012.

Wada, Y., Lo, M.-H., Yeh, P. J.-F., Reager, J. T., Famiglietti, J. S., Wu, R.-J., and Tseng, Y.-H.: Fate of water pumped from underground and contributions to sea-level rise, Nature Climate Change, 6, 777–780, https://doi.org/10.1038/nclimate3001, 2016.

Wilkinson, M. D., Dumontier, M., Aalbersberg, I. J., Appleton, G., Axton, M., Baak, A., Blomberg, N., Boiten, J.-W., da Silva Santos, L. B., Bourne, P. E., Bouwman, J., Brookes, A. J., Clark, T., Crosas, M., Dillo, I., Dumon, O., Edmunds, S., Evelo, C. T., Finkers, R.,

765   Gonzalez-Beltran, A., Gray, A. J. G., Groth, P., Goble, C., Grethe, J. S., Heringa, J., 't Hoen, P. A. C., Hooft, R., Kuhn, T., Kok, R., Kok, J., Lusher, S. J., Martone, M. E., Mons, A., Packer, A. L., Persson, B., Rocca-Serra, P., Roos, M., van Schaik, R., Sansone, S.-A., Schultes, E., Sengstag, T., Slater, T., Strawn, G., Swertz, M. A., Thompson, M., van der Lei, J., van Mulligen, E., Velterop, J., Waagmeester, A., Wittenburg, P., Wolstencroft, K., Zhao, J., and Mons, B.: The FAIR Guiding Principles for Scientific Data Management and Stewardship, Scientific Data, 3, 160 018, https://doi.org/10.1038/sdata.2016.18, 2016.

770   Woodworth, P., Hunter, J., Marcos Moreno, M., Caldwell, P., Menendez, M., and Haigh, I.: GESLA (Global Extreme Sea Level Analysis) high frequency sea level dataset-Version 2, Tech. rep., British Oceanographic Data Centre-Natural Environment Research Council, 2016.

Yin, J. and Goddard, P. B.: Oceanic Control of Sea Level Rise Patterns along the East Coast of the United States, Geophysical Research Letters, 40, 5514–5520, https://doi.org/10.1002/2013GL057992, 2013.

Yin, J., Schlesinger, M. E., and Stouffer, R. J.: Model projections of rapid sea-level rise on the northeast coast of the United States, Nature

775   Geoscience, 2, 262–266, https://doi.org/10.1038/ngeo462, 2009.